Design and catalytic studies of structural and functional models of the catechol oxidase enzyme

Journal:	*Journal of Biological Inorganic Chemistry*
Manuscript ID	JBIC-20-02-00038.R1
Manuscript Type:	Original Paper
Date Submitted by the Author:	n/a
Complete List of Authors:	Terán, Aarón; Universidad Complutense de Madrid, Quimica Inorgánica Jaafar, Aida; Complutense University of Madrid Faculty of Chemical Sciences, Departamento de Química Inorgánica Sánchez-Peláez, Ana E.; Complutense University of Madrid Faculty of Chemical Sciences, Departamento de Química Inorgánica Torralba, M. Carmen; Complutense University of Madrid Faculty of Chemical Sciences, Departamento de Química Inorgánica Gutiérrez, Ángel; Complutense University of Madrid Faculty of Chemical Sciences, Departamento de Química Inorgánica
Keywords:	Catalytic activity, Biomimetic catalysis, Cu (II) complexes
Note: The following files were submitted by the author for peer review, but cannot be converted to PDF. You must view these files (e.g. movies) online.	
gc4.cif	

TITLE

Design and catalytic studies of structural and functional models of the catechol oxidase enzyme

AUTHOR NAMES

Aarón Terán, Aida Jaafar, Ana E. Sánchez-Peláez, M. Carmen Torralba, Ángel Gutiérrez.*

AUTHOR ADDRESS

Departamento de Química Inorgánica, Facultad de Ciencias Químicas, Universidad Complutense de Madrid, Madrid 28040, Spain

CORRESPONDING AUTHOR

*E-mail: aaronter@ucm.es

ORCID Aarón Terán: 0000-0001-6126-6230

Dedicated to Professor José Antonio Campo Santillana, in memoriam

ABSTRACT

The catechol oxidase activity of three copper/bicompartmental *salen* derivatives has been studied. One mononuclear, [CuL] (**1**), one homometallic, $[Cu_2L(NO_3)_2]$ (**2**), and one heterometallic, $[CuMnL(NO_3)_2]$ (**3**), complexes were obtained by using the ligand H_2L= *N*,*N*'-bis(3-methoxysalicylidene)-1,3-propanediamine through different synthetic methods (electrochemical, chemical and solid state reaction). The structural data indicate that the metal ions disposition models the active site of *type-3* copper enzymes, such as catechol oxidase. In this way, their ability to act as functional models of the enzyme has been spectrophotometrically determined by monitorization of the oxidation of 3,5-di-*tert*-butylcatechol (3,5-DTBC) to 3,5-di-*tert*-butyl-*o*-benzoquinone (3,5-DTBQ). All the

complexes show significant catalytic activity with ratio constants (k_{obs}) lying in the range (223 - 294)×10^{-4} min^{-1}. A thorough kinetic study was carried out for complexes **2** and **3**, since their show structural similarities with the catechol oxidase enzyme. The greatest catalytic activity was found for the homonuclear dicopper compound **(2)** with a turnover value (k_{cat}) of (3.89 ± 0.05)×10^6 h^{-1}, which it is the higher reported to date, comparable to the enzyme itself (8.25×10^6 h^{-1}).

GRAPHICAL ABSTRACT

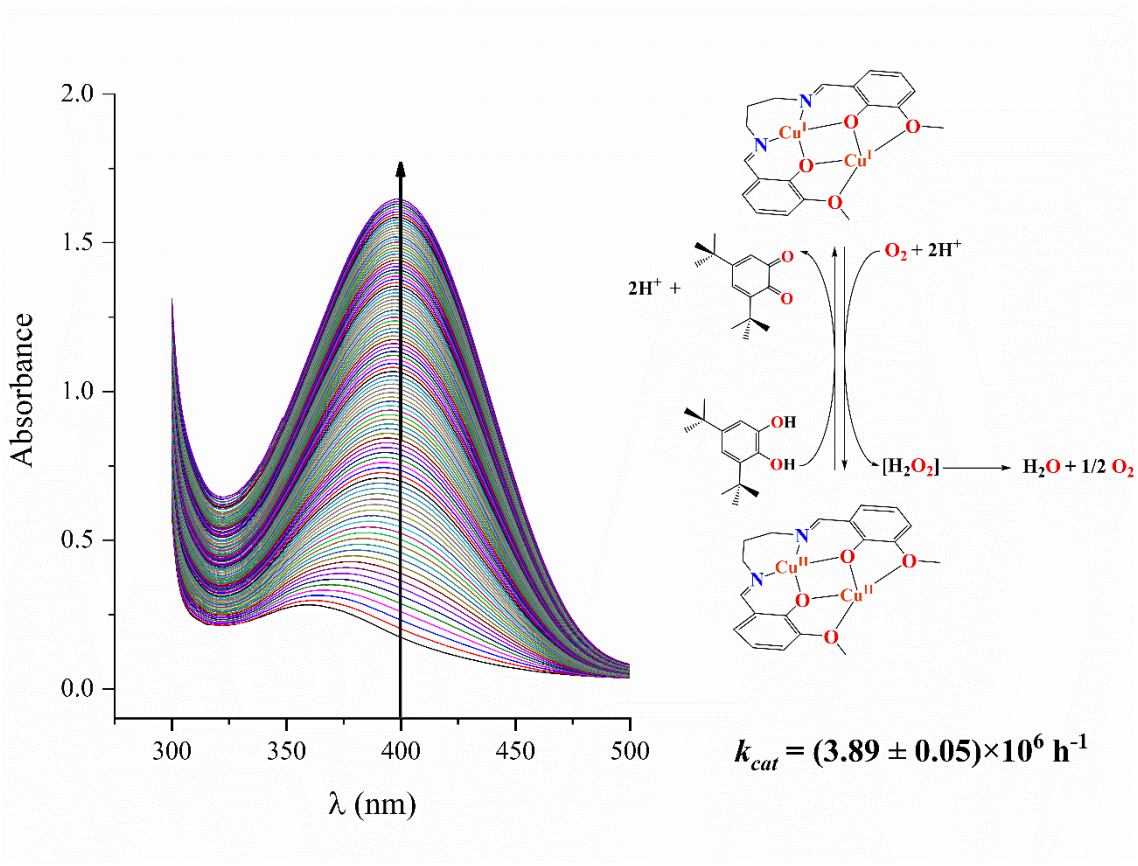

KEYWORDS

Catalytic activity, Biomimetic catalysis, Cu (II) complexes

1. INTRODUCTION

In last decades, one of the main purposes in bioinorganic chemistry focus on the synthesis and study of chemical models able to mimic the structure and function of the enzyme active sites using coordination chemistry compounds [1]. Those models are simpler and, therefore, easy to study the relationship between structure and enzymatic function in order to stablish a mechanism of the catalytic processes. Besides, in several cases, some of these reactions can be implemented in the industry with an adequate catalyst obtaining compounds under "greener" conditions [2].

Catechol oxidase enzyme is present in plants, animals, fungi and bacteria. It takes part in the conversion of a large number of *o*-catechols into the respective *o*-benzoquinones, which subsequently auto-polymerize, resulting in the formation of melanin, a dark pigment thought to protect a damaged tissue from pathogens. This enzyme is also relevant in the industry because of its uses as O_2 activator [2–4] or in medical diagnosis of human brain diseases (detection of catecholamines, noradrenaline and dopa in neurological disorders) [5].

The *type-3* active site of the enzyme consists of a dinuclear copper center where each copper is coordinated by three histidine nitrogen atoms and one hydroxo bridge, in the native *met* state [6]. Since the discovery of the nature of this active site, a great number of dicopper(II) complexes have been designed to mimic the structure and function of the enzyme [7].

The Schiff base type ligands provide great environments to obtain dinuclear copper(II) complexes. In particular, bicompartmental *salen* (*N*,*N*′-disalicylideneethylenediamine) and its derivatives can be easily synthesized by condensation of an aldehyde or ketone with a primary amine [8]. Several modifications can be introduced in this type of ligands in order to modify their electronic and structural properties such as flexibility, electronic

nature or steric characteristics resulting in an exceptionally rich coordination chemistry [9–11].

The best catechol oxidase model reported to date with copper complexes exhibit k_{cat} values around 10^4 h^{-1}, at least two orders of magnitude lower than those of the enzymes isolated from different sources (k_{cat}= 8.25×10^6 h^{-1} from *Ipomoea batatas* (sweet potatoes) [12] and k_{cat}= 5.7×10^5 h^{-1} from *Lycopus europaeu* [13]). In that sense, due to the great importance of this enzyme, it is of big interest to develop new models in order of improving their catecholase activity.

In this work, we report the synthesis and structural characterization of three structural model complexes of catechol oxidase enzyme obtained by using one symmetric bicompartmental Schiff base ligand (*N*,*N*'-bis(3-methoxysalicylidene)-1,3-propanediamine, H_2L). This ligand has an inner site, N_2O_2, formed by two imines and two phenol groups and one outer site, O_2O_2, from the two bridging phenol groups and two methoxy groups in 3,3' positions (*Fig. 1a*). The inner site is more suitable to accommodate *3d* metal ions [14–19], while the external one is capable to accept diverse metal ions such as alkali [20], alkali-earth [21], transition metals [22, 23] and lanthanides [24–26] as well as small molecules like water [27, 28] or ammonium cation [29]. We have also studied the catalytic activity of these complexes in order to check whether they can act not only as structural model but as functional models of the enzyme. The studies have been carried out using UV-Vis spectroscopy to follow the oxidation process of 3,5-di-*tert*-butylcathechol (3,5-DTBC) to 3,5-di-*tert*-butyl-*o*-benzoquinone (3,5-DTBQ) in an aerobic methanolic solution buffered at pH= 8.

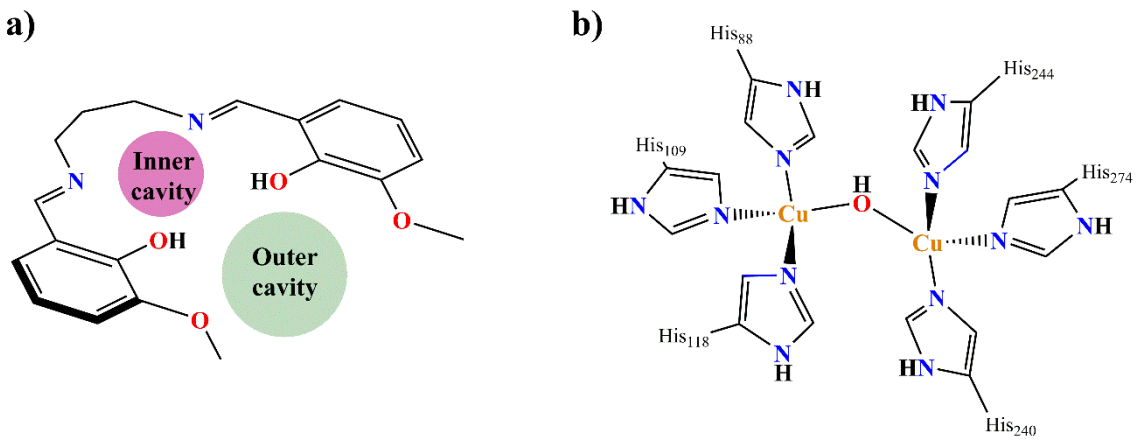

Fig. 1. Coordination environment resemblance between the bicompartmental ligand H_2L (a) and the active site of catechol oxidase enzyme (b).

2. MATERIALS AND METHODS

2.1 Synthesis of complexes

2.1.1 Synthesis of H_2L

This ligand H_2L, (*N*,*N*′-bis(3-metoxysalicylidene)-1,3-propanediamine), was obtained by previously reported procedures [30]. A mixture of 3-methoxy-2-hydroxy-benzaldehyde (4.30 g, 28 mmol) and 1,3-diaminopropane (1.2 mL, 14 mmol) in methanol (20 mL) by refluxing for six hours. A yellow powder appears on cooling. The solid was filtered off, washed with methanol and air-dried. Yield 3.67 g (77 %). Anal. $C_{19}H_{22}N_2O_4$ (342.39 $g \cdot mol^{-1}$) Calcd (%): C, 66.65; H, 6.48; N, 8.18. Found (%): C, 66.27; H, 6.32; N, 8.19. IR (cm^{-1}): 3421, 2940, 2948, 2902, 2880, 2839, 1631, 1491, 1469, 1441, 1414, 1384, 1359, 1337, 1271, 1256, 1171, 1129, 1095, 1081, 1051, 1032, 1006, 975, 961, 881, 837, 785, 742, 730, 623, 570, 507. ^{1}H-NMR (300 MHz, $CDCl_3$): δ= 13.92 ppm (s, 2H, **OH**), δ= 8.37 ppm (s, 2H, **CH**=N), δ= 7.25 – 6.80 ppm (m, 6H, **ArH**), δ= 3.91 ppm (s, 6H, **OCH_3**), δ= 3.76-3.71 ppm (td, 4H, N-**CH_2**), δ= 2.16 – 2.06 ppm (q, 2H, CH_2-**CH_2**-CH_2). UV-Vis (CH_3OH): λ_{max}/nm (ε/$dm^3 \cdot mol^{-1} \cdot cm^{-1}$)= 263 (15280), 296 (6196), 326 (3324), 420 (3321).

2.1.2 Synthesis of [CuL] (1)

H_2L (0.66 g, 2 mmol) was dissolved in methanol (140 mL) and placed in an electrochemical cell with a sacrificial copper anode and an inert platinum cathode, using Et_4NBr as electrolyte. The intensity value was set up at 40 mA and the output was 100 V. The reaction time was 2 h and 41 min at room temperature. The green solid obtained was filtered off, methanol washed and vacuum dried. The E_f value was 0.5 mol·F^{-1} which corresponds to the oxidation of metallic copper to Cu(II). Yield 0.48 g (60 %). Anal. $C_{19}H_{20}CuN_2O_4$ (403.90 g·mol^{-1}) Calcd (%): C, 56.50; H, 4.99; N, 6.94. Found (%): C, 56.42; H, 4.91; N, 6.94. IR (cm^{-1}): 3431, 3053, 2999, 2941, 2830, 1629, 1545, 1471, 1441, 1403, 1327, 1243, 1221, 1167, 1101, 1082, 1008, 977, 959, 939, 857, 786, 743, 619, 560, 452. UV-Vis (CH_3OH): λ_{max}/nm (ε/dm^3·mol^{-1}·cm^{-1})= 282 (24773), 371 (7172), 550 (197).

2.1.3 Synthesis of [$Cu_2L(NO_3)_2$] (2)

Three different procedures have been followed for the synthesis of the title compound.

i. A methanolic solution (40 mL) of $Cu(NO_3)_2·3H_2O$ (0.80 g, 3.3 mmol) was added to an stirring solution of H_2L (0.36 g, 1.1 mmol) in methanol (15 mL). The reaction mixture was stirred at room temperature for 12 h. The solid appeared as a brown powder that was filtered off and washed with methanol. Single crystals suitable for X-ray data collection were obtained by slow evaporation of the filtered solution. Yield 0.41 g (65 %).

ii. H_2L (0.17 g, 0.5 mmol) and $Cu(NO_3)_2·3H_2O$ (0.14 g, 0.56 mmol) were dissolved in methanol (105 mL) in an electrochemical cell with a sacrificial copper anode and an inert platinum cathode. The intensity value was set up at 40 mA and the output was 100 V. The reaction time was 41 min at room temperature. The product was filtered off, washed with methanol and dried. The E_f value was 0.5 mol·F^{-1}. Yield 0.13 g (43 %).

iii. A solid mixture of $Cu(NO_3)_2 \cdot 3H_2O$ (0.10 g, 0.4 mmol) and H_2L (0.14 g, 0.4 mmol) were ground for 30 min at room temperature. The mixture was suspended in methanol to extract the excess of reagents and leaving the product as a brown solid, which was filtered, washed with cold methanol and dried over P_4O_{10}. Yield 0.12 g (52 %).

Anal. $C_{19}H_{20}Cu_2N_4O_{10}$ (591.47 g·mol^{-1}) Calcd (%): C, 38.12; H, 3.50; N, 9.36. Found (%): C, 37.82; H, 3.34; N, 9.26. IR (cm^{-1}): 2993, 2949, 2925, 1627, 1613, 1559, 1519, 1494, 1477, 1466, 1440, 1422, 1409, 1384, 1353, 1335, 1307, 1297, 1245, 1233, 1199, 1173, 1101, 1079, 1070, 1015, 1011, 990, 983, 955, 934, 894, 855, 839, 805, 784, 762, 745. UV-Vis (CH_3OH): λ_{max}/nm (ε/dm^3·mol^{-1}·cm^{-1})= 226 (47027), 279 (24284), 360 (6360), 608 (78).

2.1.4 Synthesis of [CuMnL$(NO_3)_2$] (3)

This compound has been prepared following the previously reported procedure [22]. The mononuclear complex (1) (0.10 g, 0.5 mmol) was dissolved in MeOH:MeCN (1:4) (125 mL), $Mn(NO_3)_2 \cdot 4H_2O$ (0.06 g, 0.5 mmol) was added and the resulting solution was stirred for 0.5 h. After four days of slow evaporation at low temperature, a dark green powder and single crystals suitable for X-ray data collection were obtained. The product was filtered off, washed with cold methanol and dried in vacuum. Yield 0.19 g (66 %). Anal. $C_{19}H_{20}CuMnN_4O_{10}$ (582.87 g·mol^{-1}) Calcd (%): C, 39.15; H, 3.46; N, 9.61. Found (%): C, 39.36; H, 3.58; N, 9.27. IR (cm^{-1}): 1617, 1561, 1472, 1445, 1384, 1302, 1236, 1172, 1101, 1073, 1030, 988, 953, 855, 786, 745, 638, 574, 539, 466. UV-Vis (CH_3OH): λ_{max}/nm (ε/dm^3·mol^{-1}·cm^{-1})= 226 (44254), 276 (19559), 356 (4630), 618 (33).

2.2 Physical Methods and Materials.

All chemicals of analytical-grade were purchased from Sigma-Aldrich and used without further purification.

Elemental analysis (carbon, hydrogen and nitrogen) were carried out by the Microanalytical Service of the Universidad Complutense de Madrid (UCM) using a LECO CHNS-932 analyser. FTIR spectra (4000-650 cm^{-1}) of solid powder samples were recorded using a Perking Elmer spectrophotometer with a universal ATR accessory and FTIR KBr-dispersion spectra (4000-400 cm^{-1}) were recorded using a THERMO NICOLET 200 spectrophotometer. Mass spectra were recorded using electrospray ionization (ESI-MS) in DMSO and MeOH with the HCTultraPTM Discovery System mass spectrometer equipped with a conventional ESI source. ^{1}H-NMR spectra were collected in the UCM Nuclear Magnetic Resonance Service using a Burker AVIII300 (300 MHz) spectrophotometer. Electronic spectra in oxygenated methanol (200-1000 nm) were registered in a Cary-5G spectrophotometer. The measurements of the catalytic oxidation of 3,5-di-*tert*-butylcatechol (3,5-DTBC), were carried out in a JASCO V-630 spectrophotometer at a constant wavelength of 400 nm under aerobic conditions at 20 ºC and in buffered solution at pH= 8 with tris(hydroxymethyl)aminomethane (Tris). Variable-temperature magnetic susceptibility measurements in the temperature range 2-300 K were performed on a Quantum Design MPMSXL SQUID magnetometer using a constant magnetic field of 0.5 T. All susceptibility data were corrected for the diamagnetic contribution of the sample holder, while the molar diamagnetic corrections from the sample were calculated using the Pascal constants. Cyclic voltammetry (CV) measurements were performed using an EmStat3 blue potentiostat controlled by PSTrace software. A three-electrode assembly comprising a gold working electrode, platinum auxiliary electrode and Ag/AgCl electrode as reference electrode were used. The cyclic voltammetry study was carried out at room temperature in MeCN:H_2O (2:1) solution under Argon with 50 mM Tris buffer (pH= 8) at a scan rate of 50 $mV \cdot s^{-1}$ in a potential range from +0.8 V to -0.8 V.

2.3 Crystallographic studies.

A good quality crystal of (**2**) was directly collected from the reaction vessel and mounted on a Bruker Smart-CCD diffractometer using graphite monochromated Mo Kα radiation (λ= 0.71073 Å) operating at 50kV and 25 mA at 293 K. Data were collected over a reciprocal space hemisphere by combination of three exposure sets. Each frame exposure time was 20 s covering 0.3º in ω. The cell parameters were determined and refined by least-squares fit of all reflections collected. The first 50 frames were recollected at the end of the data collection to monitor crystal decay, and no appreciable decay was observed. The structure was solved by direct methods and refined by applying full-matrix least-squares on F^2 with anisotropic thermal parameters for the non-hydrogen atoms. The hydrogen atoms were included with fixed isotropic contributions at their calculated positions determined by molecular geometry. All the calculations were carried out using SHELXT program for solution and SHELXL for refinement [31] working into the OLEX2 software package program [32]. A summary of the fundamental data can be found in the supplementary material *Table S1*.

2.4 Catalytic activity and kinetic studies

Catecholase-like activity and kinetic studies of complexes **1-3** were evaluated in aerobic condition spectrophotometrically by monitoring the oxidation of 3,5-DTBC to 3,5-DTBQ at 400 nm as a function of time. The reaction was studied in a thermostated cell with 1 cm path length at 20.0 ± 0.1 °C. The solvent used to prepare all solutions was Tris buffer (100 mM, pH 8) in methanol medium saturated with atmospheric dioxygen during several minutes.

For catalytic activity studies, 2×10^{-5} M solutions of complexes **1-3** were treated with 2×10^{-3} M solutions of the substrate 3,5-DTBC. The reaction progress was followed by UV/Vis spectroscopy observing the increase in the characteristic quinone (3,5-DTBQ)

absorption band at 400 nm. The data were taken at intervals of 60 s and the conversion was measured up to 60 min in each case. All data were fixed to a first-order kinetic according to equation 1, where A_∞ denotes absorbance at $t = \infty$, A_t is the variation absorbance value with time and k_{obs} is the rate constant.

$$log\left(\frac{A_\infty}{A_\infty - A_t}\right) = k_{obs} \cdot t \quad (1)$$

Enzymatic kinetic experiments for the oxidation of 3,5-DTBC to 3,5-DTBQ were performed using complex **2** and **3** as catalysts. The experimental procedure was carried out by the initial rate method monitoring by UV-Vis spectroscopy. The experiments were carried out by keeping constant the final catalyst concentration at 2×10^{-5} M and changing the substrate concentration between 2×10^{-3} to 2×10^{-2} M.

3. RESULTS AND DISCUSSION

3.1 Synthesis of complexes

The synthetic procedures followed in this work are summarized in *Scheme 1*.

The mononuclear complex [CuL] **(1)** has been obtained by an electrochemical procedure, an unusual synthetic route for this type of compound, where a copper wire electrode is oxidized by an electric current to form copper (II) ions that coordinate into the inner cavity of the anionic bicompartmental ligand. This procedure allows a precise stoichiometric control of the reacting copper(II) amount, obtaining purer derivatives with a lower formation of by-products.

The efficiency of the electrochemical process is 0.5 $mol \cdot F^{-1}$, indicative of a two electron transfer according to the following half-reactions:

$$\text{Anode: } L^{2-} + Cu^0 \rightarrow [CuL] + 2e^-$$

$$\text{Cathode: } H_2L + 2e^- \rightarrow H_2\,(g) + L^{2-}$$

The homonuclear $[Cu_2L(NO_3)_2]$ **(2)** has been synthetized by three different routes:

i. Electrochemical synthesis in presence of excess $Cu(NO_3)_2 \cdot 3H_2O$.

ii. One-pot chemical reaction by mixing methanolic solutions of H_2L and $Cu(NO_3)_2 \cdot 3H_2O$ in a 1:2 stoichiometric ratio.

iii. Solid state grinding of H_2L and $Cu(NO_3)_2 \cdot 3H_2O$ in a 1:2 ratio.

All procedures lead to similar results in purity and yield of the dinuclear derivative.

The heteronuclear derivative, **3**, can only be obtained in good yields by reaction of methanolic solutions of **1** with $Mn(NO_3)_2 \cdot 4H_2O$. The use of other synthetic procedures lead to a competition between the Cu(II) and Mn(II) ions to occupy the coordinative cavities of the *salen* ligand, the main product being **2**.

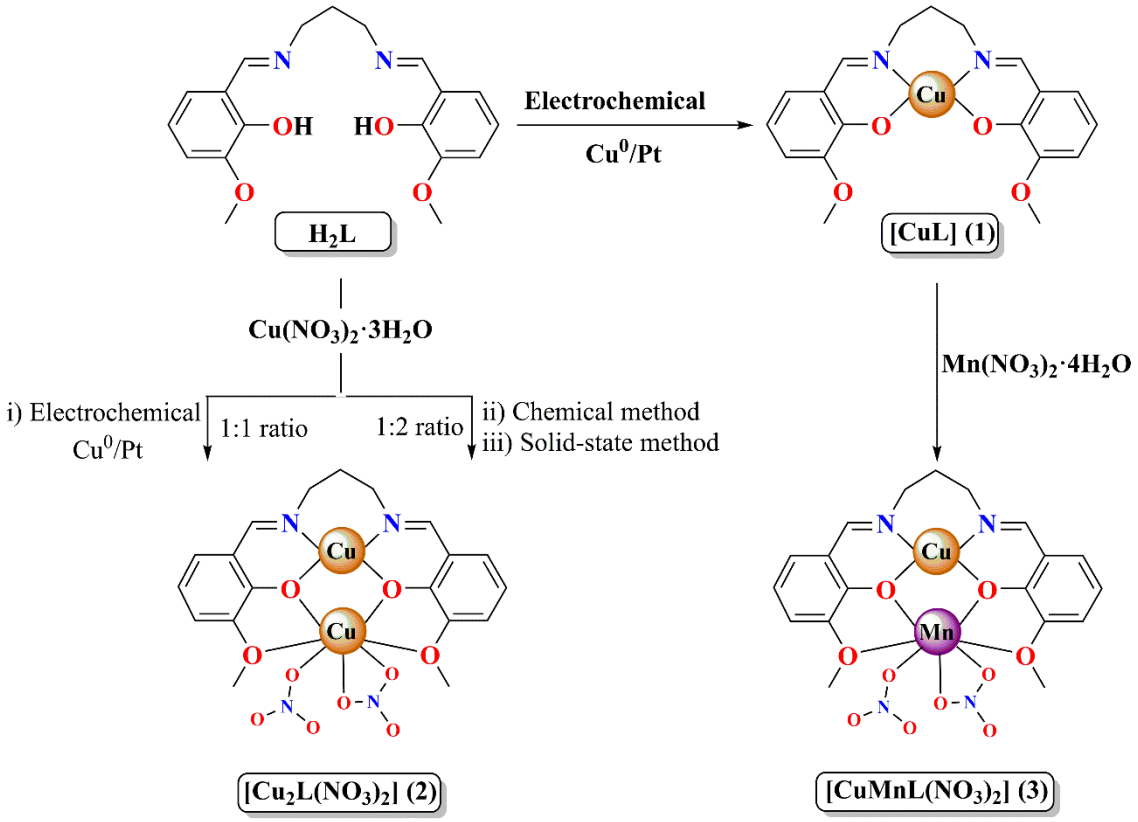

Scheme 1. Synthetic routes used for the preparation of complexes **1**-**3**.

3.2 Infrared spectra

The IR spectra indicate that the coordination of a metal center to the *salen* ligand slightly shifts the characteristic vibration bands, ν(C=N)= 1630 cm^{-1}, $\nu(C\text{-}O)_{phenoxo}$= 1255 cm^{-1}

and ν_s(C-OCH_3)= 1081 cm^{-1}. Thus, these bands appear respectively at 1629, 1239 and 1070 cm^{-1} for **1**, 1613, 1245 and 1070 cm^{-1} for **2** and 1617, 1246 and 1070 cm^{-1} for **3**. The shift to lower frequencies is indicative of the lower electron density on the donor atoms because of the coordination of the metal atoms [33]. The two latter compounds also show characteristic bands around 1470, 1310 and 1030 cm^{-1} associated to ν(N=O), $\nu_{as}(NO_2)$ and $\nu_s(NO_2)$, respectively, which are indicative of the presence of coordinated nitrate groups [34] (see supplementary material *Figure S1*).

3.3 Electronic spectra

The electronic spectrum for the ligand, H_2L, shows three bands in the 260-330 nm region that are ascribed to intraligand $\pi \rightarrow \pi^*$ and $n \rightarrow \pi^*$ transitions. Additionally, the ligand shows an intense absorption band at 420 nm, assigned to a charge transfer between the ligand and the methanol solvent (MSCT), since this band was not observed when the spectra was collected in acetonitrile solution. The formation of the complexes causes a bathochromic shift of the intraligand transitions along with the appearance of a low-intensity absorption band centred at 600 nm that can be assigned to a *d-d* transition for the copper(II) ion due to the $^2T_{2g} \leftarrow {}^2E_{2g}$ transition. In the dinuclear complexes a charge transfer between the metal ion and the ligand (MLCT) at about 360 nm for **2** and 356 nm for **3** is also observed. A board low-intensity absorption band at 608 nm for the Cu-Cu complex and 618 nm for the Cu-Mn one is also attributed to the *d-d* transition of the copper(II) ion [35] (see supplementary material *Figure S2*).

3.4 X-ray crystal structure of (2)

Single crystals suitable for X-ray diffraction have been obtained from methanolic solutions of the dinuclear complexes.

The crystal structure of **2** indicates that it is isomorphous with the previously characterized complex **3** (*Fig. 2*) [22]. Both complexes show a copper(II) ion coordinated

to the inner cavity, N_2O_2, in a square-planar geometry. The presence of a second coordination site, O_2O_2, allows the coordination of a second metal ion, copper(II) in **2** or manganese(II) in **3**. In both cases, this ion is heptacoordinated by the four oxygen atoms from the outer site of the ligand and by three oxygen atoms from two nitrate anions, in a bidentate and monodentate fashion. The bond distances between the copper ion and the donor atoms in the inner cavity are very similar, about 1.9 Å, in both complexes. The difference in size of the metal ion located in the outer cavity results in small differences in the metal-oxygen distances (2.41-2.42 Å for the Cu-Cu derivative and 2.37-2.38 Å for the Cu-Mn one), leading to metal-metal separations of Cu···Cu= 3.232(1) Å and Cu···Mn= 3.322(1) Å respectively. The former distance is very similar to the Cu···Cu distance observed in the *met* state of catechol oxidase enzyme (3.032 Å). A comparison between the coordinative environment of the dinuclear complexes and that of the active site of *met* state of this enzyme is observed in *Figure 3*.

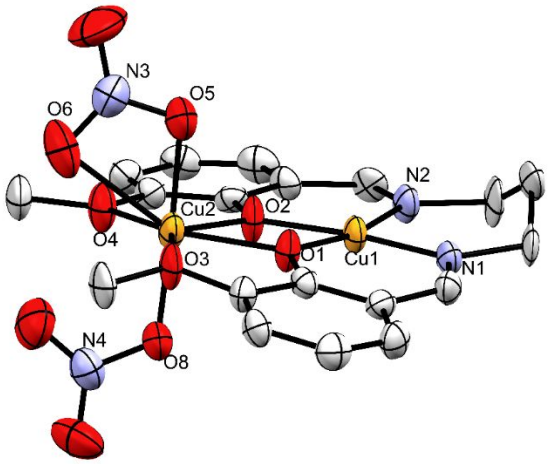

Fig. 2. ORTEP view (50% probability ellipsoids) and labelling scheme of the asymmetric unit for **2**.

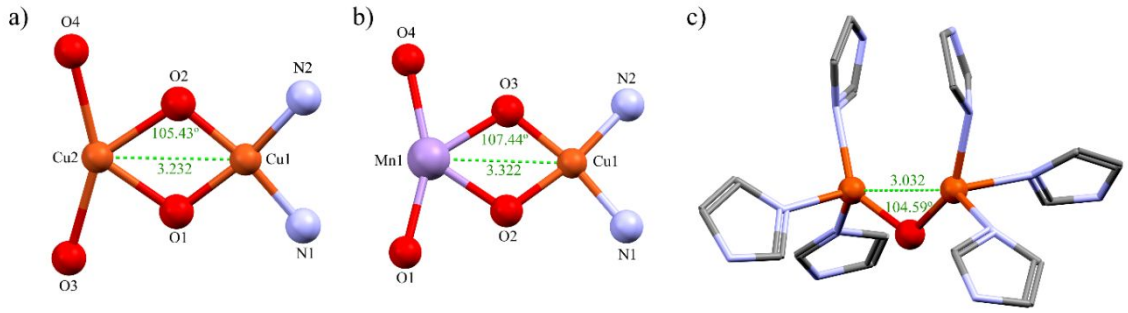

Fig. 2. Metal-metal distances and angles of dinuclear complexes, **2** (**a**) and **3** (**b**), and the coordination sphere of the dinuclear copper(II) centre of catechol oxidase from sweet potato in the *met* state (PDB ID: 1BT3) (**c**).

3.5 Magnetic properties

The magnetic susceptibility data for **2** and **3** have been measured in the temperature range 2-200 and 2-300 K respectively. The temperature dependence of the χT values has been plotted in *Figure 4* for the two complexes.

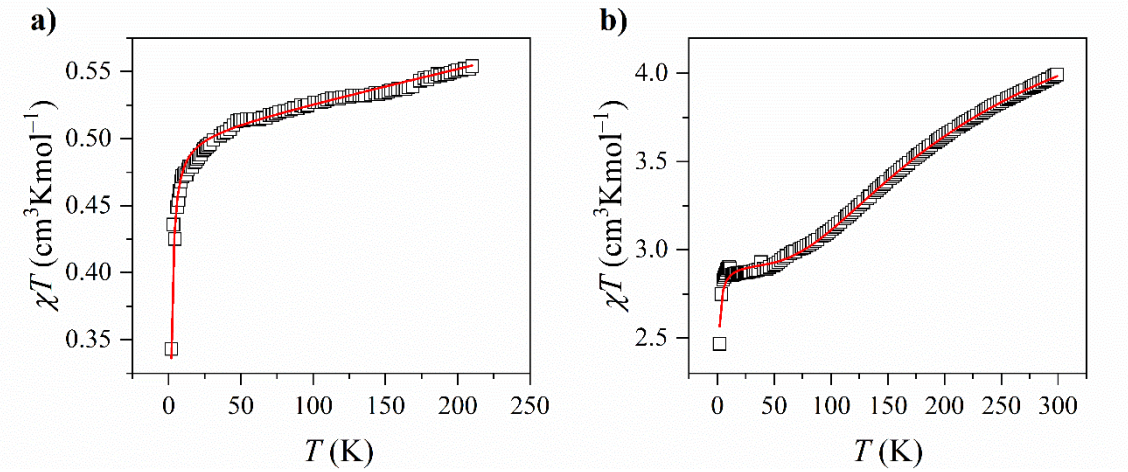

Fig. 4. Temperature dependence of χT for complexes a) **2** and b) **3**. The solid lines represent the fit of the data using the parameters described in the text.

The high temperature value of χT for **2** (*Fig. 4a*) is 0.554 cm^3Kmol^{-1}, below the expected value for two isolated S= ½ spins (0.75 cm^3Kmol^{-1}). On cooling, the χT values decrease to a minimum value of 0.343 cm^3Kmol^{-1} at 2 K. This behaviour can be interpreted in terms of an antiferromagnetic coupling between the two copper(II) ions in the same molecular unit. In this sense, the magnetic data for the dicopper complex have been fitted to Heisenberg´s dimers model according to Hamiltonian $H= -J \cdot S_1 \cdot S_2$, where J is the

coupling constant between both spins, with the addition of a temperature independent paramagnetism term. The best fit (solid line) was obtained when g= 2.305(2), J= -1.45(3) cm^{-1} and $N\alpha$= 2.7(1)×10^{-4} cm^3mol^{-1}, this results agree with the antiferromagnetic behaviour between the two metal ions.

Compound **3** shows a similar behaviour (*Fig. 4b*), with a room temperature χT value at of 3.99 cm^3Kmol^{-1}, lower than the expected for one S= ½ and one S= $^5/_2$ independent spins (4.38 cm^3Kmol^{-1}). The χT values decrease on cooling until ca. 40 K, when they reach a plateau at 2.89 cm^3Kmol^{-1}, very close to the expected value of 3.00 cm^3Kmol^{-1} for the two spins coupling antiferromagnetically. Below 15 K the χT values decrease once more to a minimum value of 2.47 cm^3Kmol^{-1} at 2 K; this fact can be attributed to the zero field splitting of the manganese ion, observable at very low temperatures, indicative of a small anisotropy distortion in the metal environment. In order to simplify the fitting, we have treated the data in two steps:

The evaluation of the zero field splitting contribution for the manganese has been evaluated by fitting the data below 30 K, with the use of the Hamiltonian $H= D\cdot S_z^2$, where D is the zero field splitting parameter for the manganese ion. The best fit corresponds to g_{Mn}= 1.962(2) and D= 1.52(7) cm^{-1}.

In a second step, the whole set of data were fitted, using a Heisenberg's dimers model and the zero field splitting correction for the Mn(II) cation anisotropy, along with a temperature independent paramagnetism term, usually present when the Cu(II) ion is involved. The resulting Hamiltonian was $H= -J\cdot S_{Cu}\cdot S_{Mn} + D\cdot S_z^2$, where J is the coupling constant between copper and manganese ions. The g_{Mn} and D values obtained from the previous fitting where kept constant and the fit (solid line in *Fig. 3*) affords the final values g_{Cu}= 2.350(2), J= –70.6(5) cm^{-1} and $N\alpha$= 4.6(2)×10^{-4} cm^3mol^{-1}, as expected for the antiferromagnetic coupling predicted between the two metal spins.

3.6 Catechol oxidase activity

The synthesized complexes in this research have been designed as structural and functional models of the catechol oxidase enzyme, so it is necessary to evaluate their ability to oxidize a catechol (3,5-DTBC) to the corresponding quinone (3,5-DTBQ). The reaction progress was followed by UV/Vis spectroscopy (*Fig. 5*) observing the increase in the characteristic quinone (3,5-DTBQ) absorption band at 400 nm as function of time in all three cases (see supplementary material *Figure S3*) [36][3].

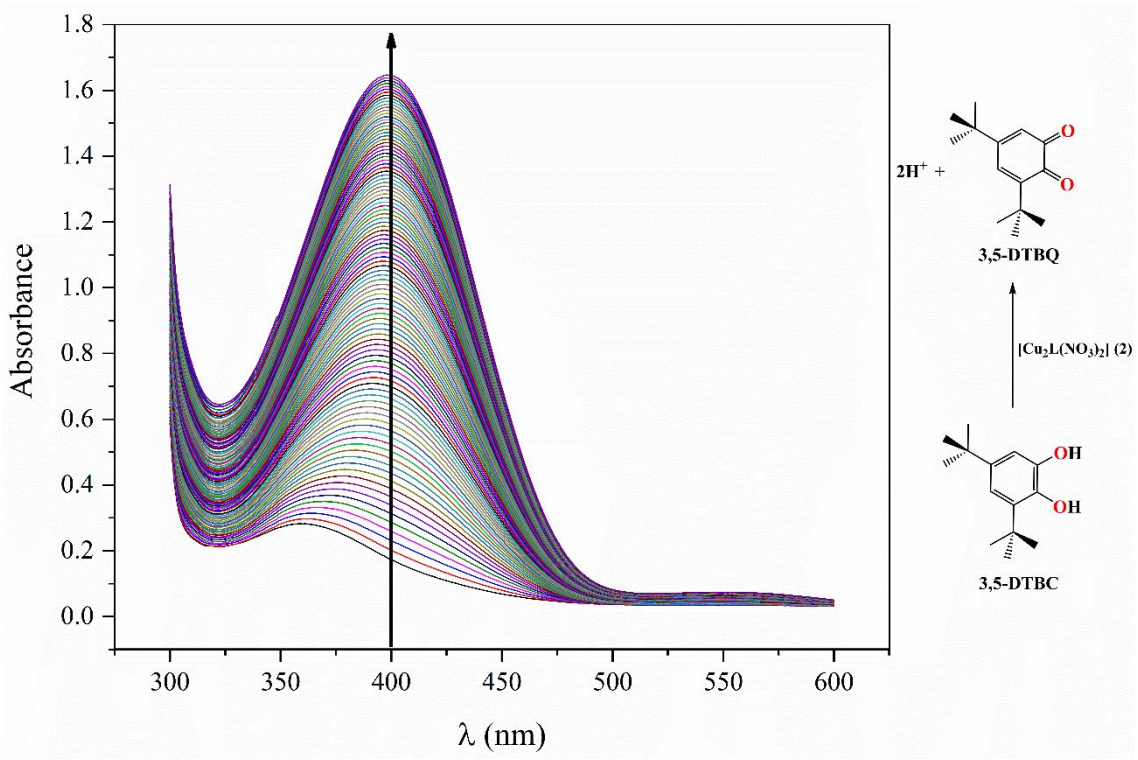

Fig. 5. Variation of 3,5-DTBQ absorbance at 400 nm after addition of complex **2**. The spectra were recorded at intervals of 60 seconds during 60 min.

As a previous step, to take into account the possible autoxidation of the catechol, different blank experiments were performed. The autoxidation of the 3,5-DTBC substrate was measured in the absence of Tris buffer and without oxygenation of the solvent and checked that the autoxidation process does not occur if the medium has not been previously oxygenated and that the highest autoxidation rate was obtained when the pH was buffered at 8.

In all three complexes, the k_{obs} values for a first-order kinetic indicate a remarkable catalytic oxidation process to form the quinone (*Table 2*).

Table 2. Values of k_{obs} obtained by using the complexes described in this work as catalysts.

Catalyst	[C] (mol/L)	k_{obs} (min^{-1})
1	2×10^{-5}	$(258 \pm 4)\times10^{-4}$
2	2×10^{-5}	$(294 \pm 4)\times10^{-4}$
3	2×10^{-5}	$(282 \pm 2)\times10^{-4}$

The obtained ratio constant values are of the same magnitude order, making difficult the identification of the complex having the best catalytic activity and the observation of what structural and compositional differences improve or fall away the catalytic process. For this reason, an evaluation of the conversion percentage of catechol to quinone was made in order to check which compound shows the best catalytic behaviour. To do this, a calibration curve was made using methanol-oxygenated 3,5-DTBC solutions buffered at pH 8 at three different concentrations, 0.005 M, 0.010 M and 0.015 M. The calibration plot allows the interpolation of the amount of quinone formed in the presence of the catalyst during the first 30 minutes of reaction. The UV-Vis absorbance at 400 nm for each solution was recorded after 24 h to ensure that all 3,5-DTBC had been converted to 3,5-DTBQ. The results are shown in *Figure 6*.

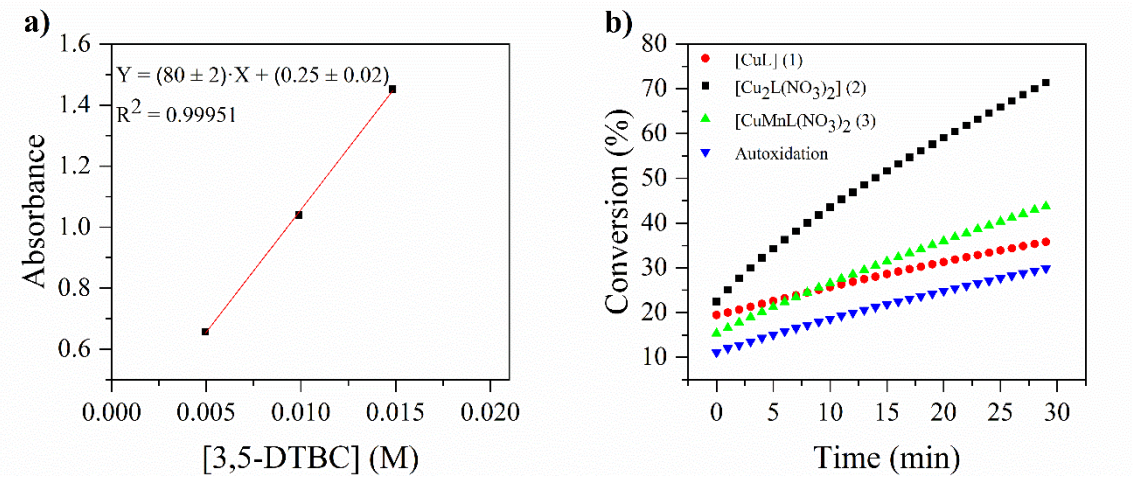

Fig. 6. a) Calibration curve of 3,5-DTBC. b) Percentage conversion of 3,5-DTBC to 3,5-DTBQ in the presence of the catalysts, **1** (**red**), **2** (**green**), **3** (**black**) and autoxidation (**blue**) during the first 30 min reaction time.

The presence of any of the three metallic compounds improves the catalytic process relative to the autoxidation process. The dinuclear compounds have a better catalytic activity than the mononuclear complex and the homonuclear dicopper derivative shows the best behaviour, since it is the most structural and compositionally analogous to the active site of catechol oxidase enzyme, which it is a *type-3* copper enzyme.

According to these results, the enzymatic kinetic study was carried out with the dinuclear compounds, **2** and **3**, because of their quick conversion processes. These compounds have been chosen in order to elucidate a possible mechanism involved in the catalytic process as well, using two analogue compounds that show differences in the composition of the active site.

Enzymatic kinetic experiments for the oxidation of 3,5-DTBC to 3,5-DTBQ were performed using **2** and **3** as catalysts, setting the final concentration at 2×10^{-5} M. The initial rate (V_o) is calculated for each substrate concentration (between 2×10^{-3} to 2×10^{-2} M) from the slope of the first order fitting data at the beginning of the reaction (only the first three measurements), when the reverse reaction is insignificant.

The obtained data were analysed using the Michaelis-Menten approach of enzymatic kinetic. The kinetic parameters, V_{max}, K_M and k_{cat}, were calculated from the Lineweaver-

Burk double reciprocal plot. The observed initial rate (V_o) versus the concentration of 3,5-DTBC plot and the Lineweaver-Burk plot for **2** and **3** are shown in *Figure 7*.

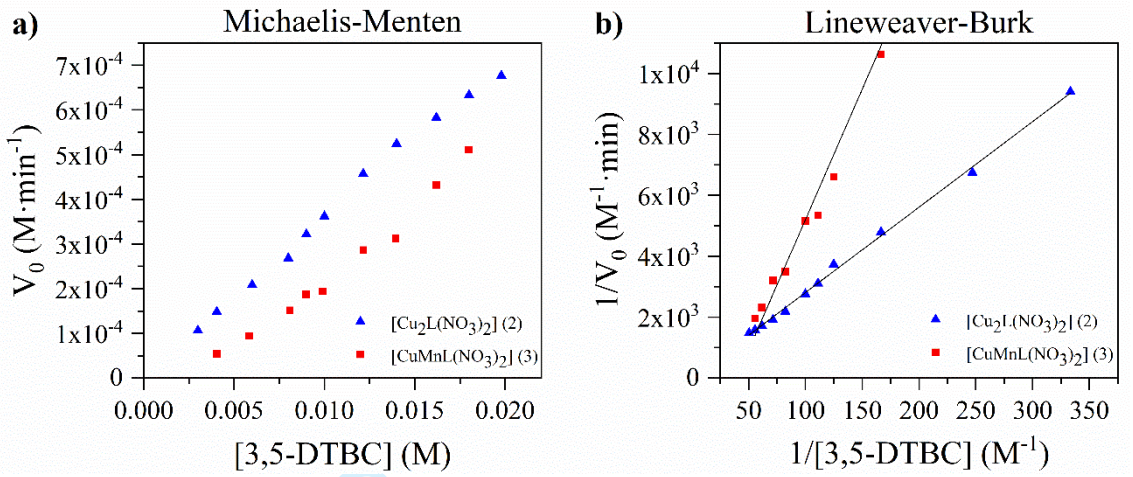

Fig. 7. a) Plot of initial rate vs. substrate concentration for the oxidation of 3,5-DTBC by complexes **2** (**red**) and **3** (**blue**). b) Lineweaver-Burk plot of complexes **2** (**red**) and **3** (**blue**).

The typical asymptotic representation of the Michaelis-Menten kinetic plot was not observed in *Figure 7a* because the maximum rate, V_{max}, is not reached. This parameter represents the amount of substrate molecules converted into the product by an enzyme molecule per unit time when the enzyme is fully saturated with substrate, so in this case the saturation of the catalysts is not achieved at the measured substrate concentrations indicating that the catalytic process must occur very quickly. The Michaelis constant (K_M), which it is inversely related with x-intercept of the graphs (*Fig. 7b*), represents the substrate concentration at half-maximum reaction rate and it is dependent on both the enzyme and the substrate, as well as on conditions such as temperature and pH. K_M is correlated with the dissociation constant of the enzyme-substrate complex, so a higher value means a low affinity in the enzyme-substrate complex.

The kinetic parameters for both complexes are summarized in *Table 3*. The higher K_M and k_{cat} values found for the dicopper derivative suggest the best catalytic behaviour for this compound.

Table 3. Kinetic parameters for the dinuclear complexes as catalysts.

[Catalyst] (M)	V_{max} (M·min^{-1})	K_M (mM)	k_{cat} (h^{-1})	k_{cat}/K_M (mM^{-1}·h^{-1})
2	0.039	36.6 ± 0.6	(3.89 ± 0.05)×10^6	106059
3	0.003	25 ± 3	892 ± 7	36

A study of the pH influence on the catalytic process has been carried out for compound **2**. The enzymatic kinetic experiments were performed at pH= 7 in the absence of buffer. In this case the k_{cat} value obtained was (2.93 ± 0.03)×10^4 h^{-1}, one order of magnitude lower than in the buffered experiment. These kinetic parameters are consistent with an improvement of the catalytic activity associated with a greater substrate-catalyst affinity favoured by the coordination of the deprotonated catechol to the copper(II) metal ions. As observed in *Figure 8* there is a substantial increase of nearly 30 % in the substrate oxidation after 30 minutes of reaction with the increase of pH.

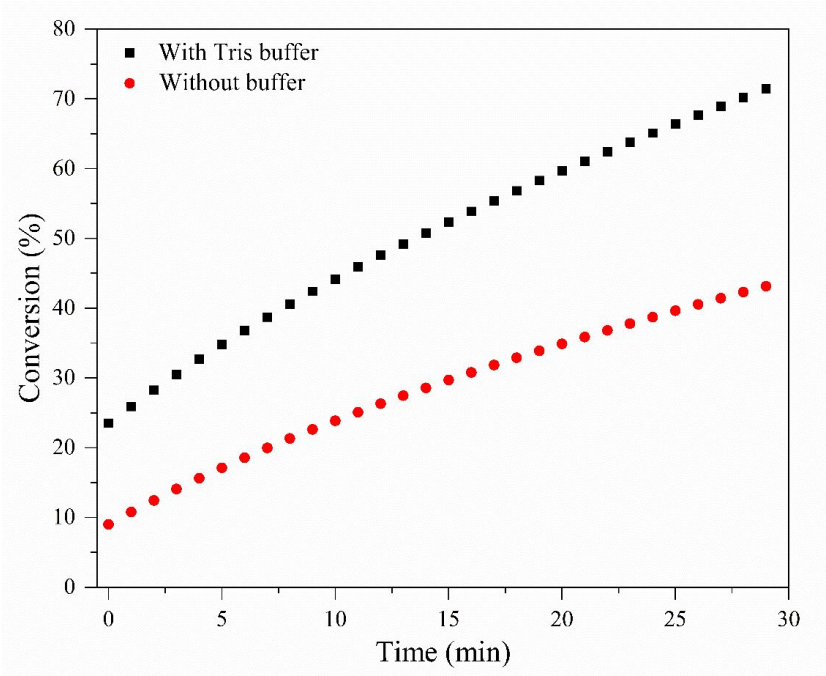

Fig. 8. Ratio of 3,5-DTBC conversion in Tris buffer medium (**black**) and without buffer (**red**) for **2**. Catalyst to 3,5-DTBC molar ratio 1:400.

Through comparison with published catalytic constant (K_M and k_{cat}) values for other metal compounds with similar catechol oxidase activity (summarized in *Table 4*), it is clear that **2** is one of the best catalyst models for this oxidation process and that the k_{cat} value is one

of the highest reported, being comparable to that measured for the catechol oxidase enzyme.

Table 4. Values of K_M and k_{cat} reported for different compounds with Schiff base ligands showing catechol oxidase activity.

Metal	Solvent	K_M (mM)	k_{cat} (h^{-1})	Ref.
Dinuclear Ni(II)	[a]	0.3	1.44×10^4	[37]
Dinuclear Cu(II)	[a]	1.7 – 2.3	$(1.08 – 3.24)\times10^4$	[38][39]
	[b]	1.09 – 9.7	$(0.0167 - 2.16)\times10^4$	
Dinuclear Mn(III)	[b]	0.9 – 3.7	$(2.41 – 3.60)\times10^3$	[5]
Mononuclear Mn(III)	[b]	0.7 – 8.3	$(0.17 – 1.80)\times10^4$	
	[a]	0.1 – 4.2	$(2.47 – 7.20)\times10^3$	
Mononuclear Mn(II)	[c]	9.52	3.10×10^6	[40]
Dinuclear Cu(II) (**2**)	[a]	36.6	3.89×10^6	This work

[a] MeOH, [b] CH_3CN, [c] DMF

This behaviour can be related to the fact that **2** is formed by a flexible ligand capable of accommodating two metal centers with a suitable Cu···Cu distance. One of these centers has coordinative vacancies while the other is coordinated to two nitrate ligands, easily displaced, favouring the coordination of a bridging catechol molecule during the catalytic process.

In the case of the Cu-Mn compound, where the only difference with the dicopper complex is the presence of a manganese (II) atom of the outer cavity, the percentage conversion values are very low. So, it can be deduced that the presence, in the case of **3**, of a second metal ion does not have a prodigious influence on the catalytic process because of the low tendency of Mn(II) to be reduced, preventing a more efficient catalytic process.

A plausible mechanism for the catalytic process using complex **2** is given in *Scheme 2*. In a first step, the 3,5-DTBC displaces one nitrate ligand from the coordination sphere of the Cu(II) ion located in the outer cavity and coordinates to the two metal ions [6][41, 42]. Electrospray ionization mass spectrometry (ESI-MS) measurements of compound **2**

detected a peaks at *m/z* = 232.9 $[M - 2NO_3]^{2+}$, 271.9 $[M - 2NO_3 + DMSO]^{2+}$ and 527.9 $[M - NO_3]^{+}$ (see supplementary material *Figure S5*). In addition, the UV-Vis measurements indicate clear differences between the solution spectra of **1** and **2**. Both facts clearly demonstrate the stability of the dinuclear derivative, both in solid state and solution, and it can be assumed that the second metal ion remains stable on the ligand outer cavity, its presence being crucial in the catalytic process.

The oxidation process of 3,5-DTBC to 3,5-DTBQ by transfer of two electron from the two Cu(II)/Cu(II) active site causes their reduction to Cu(I)/Cu(I). Once the quinone is uncoordinated, the interaction with molecular O_2 from the reaction medium produces the reoxidation of the dimetallic core giving rise to water molecules and regenerating the catalyst. The catalytic mechanism described for the most compounds that have catechol oxidase activity shows the formation of hydrogen peroxide (H_2O_2) in the catalysis process [7]. In this case, an iodometry was carried out to detect H_2O_2 during the 3,5-DTBC oxidation but no hydrogen peroxide was observed. This fact can either indicate that hydrogen peroxide was not formed and the reaction would directly proceed to the formation of water or, more probably in our opinion, that we were unable to detect the hydrogen peroxide since it would disproportionate very fast in the reaction media. According to the literature on the catalytic mechanism for cobalt and manganese compounds, the ROS involved mechanism has not been probed overall and it is supported the formation of water [43–46]. This may be because Mn and Co compounds are remarkable for carrying out the fast decomposition of H_2O_2 which leads to the formation of H_2O and O_2 [47, 48]. Chaudhuri *et al*. showed that lowering temperature (-25 ºC) can help to slow down the decomposition of H_2O_2 allowing its detection [46].

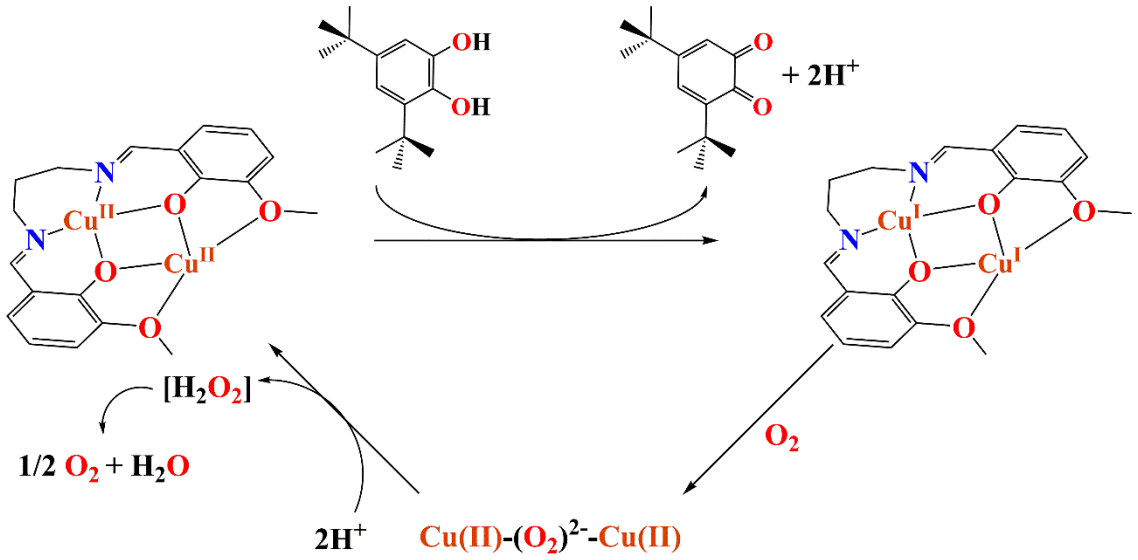

Scheme 2. Proposed mechanism for the oxidation process of 3,5-DTBC to 3,5-DTBQ.

Due to the ligand flexibility, a distortion of the coordination environment of the copper (inner or outer) from a square planar geometry to pseudo-tetrahedral is possible, through a rotation of the propylene spacer which it would facilitate the stabilization of Cu(I) ion. Cyclic voltammetric measurements have proven that the redox behaviour of **2** (*Fig. 9*) is reversible in the reaction conditions. The voltammogram plot shows two reduction peaks at -0.01 V and -0.63 V and two oxidation peaks at -0.32 V and 0.08 V, respectively. These pseudo-reversible processes can by assigned to the successive reductions from Cu(II) to Cu(I) of the metal ions. The peak centred at 0.04 V would correspond to the copper located in the inner cavity, coordinated to stronger donor atoms, while the process centred at -0.47 V can be attributed to the metal ion in the outer (O_2O_2) cavity. This result suggests a redox behaviour for this species compatible with the activity of the catecholase metal site.

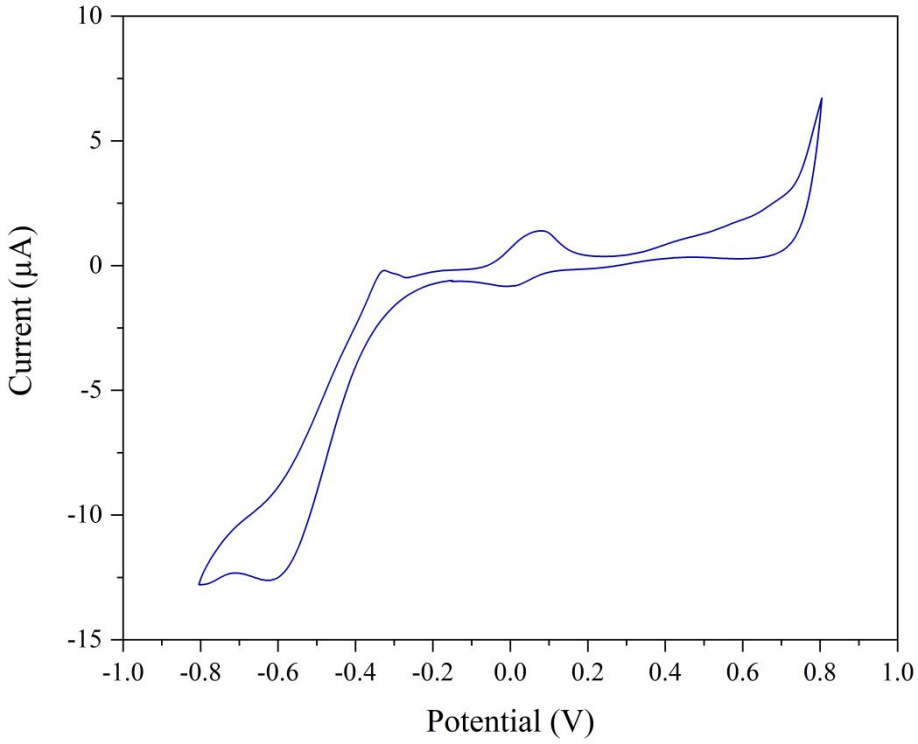

Fig. 9. Cyclic voltammogram of complex **2** in MeCN:H_2O (2:1) solution.

4. CONCLUSIONS

In summary, three complexes using a symmetrical bicompartmental Schiff base ligand, one mononuclear and two dinuclear (homo- or heterometallic) were synthesized, characterized and their catechol oxidase activity was studied. The catalytic activity of all three complexes was monitored by UV-Vis spectroscopy using the Michaelis-Menten approach to calculate their kinetic parameters complex. The obtained data suggest that the best catalytic behaviour was observed for the homonuclear derivative $[Cu_2L(NO_3)_2]$ (**2**) since this species provides the highest conversion rates and its k_{cat} value, $(3.89 \pm 0.05)\times10^6$ h^{-1}, is the highest turnover number reported to date for this catalytic process. This excellent behaviour can be related to the structural similarities observed between the Cu-Cu active site of this compound and that of the catechol oxidase enzyme. This similarity allows us to propose for this catalytic process a mechanism similar to that reported for the enzyme.

SUPPLEMENTARY INFORMATION

CCDC 1977371, contains the supplementary crystallographic data for $[Cu_2L(NO_3)_2]$. These data can be obtained free of charge via http://www.ccdc.cam.ac.uk/conts/retrieving.html, or from the Cambridge Crystallographic Data Centre, 12 Union Road, Cambridge CB2 1EZ, UK; fax: (+44) 1223-336-033; or e-mail: deposit@ccdc.cam.ac.uk.

Crystallographic parameters of **2**, Infrared and UV/Vis spectra of $\mathbf{H_2L}$ and complexes **1-3**, variation of 3,5-DTBQ absorbance at 400 nm and first-order kinetic fitting for complexes **1-3** and ESI-MS spectrum of **2** (**Table S1**, **Figure S1, S2, S3, S4** and **S5** respectively).

ACKNOWLEDGMENTS

The authors grateful acknowledge the Spanish Ministry of Economy and Competitiveness (MINECO/FEDER) for financial support (project CTQ2015-63858-P) and Comunidad de Madrid (project S2017/BMD-3770-CM). One of us (Aarón Terán) acknowledge Comunidad de Madrid (project S2017/BMD-3770-CM) for a predoctoral grant.

DECLARATIONS

The manuscript was written through contributions of all authors. All authors have given approval to the final version of the manuscript. The authors declare no competing financial interest.

REFERENCES

1. Sureshbabu P, Junaid QM, Upadhyay C, et al (2019) Di and tetranuclear Cu(II) complexes with simple 2-aminoethylpyridine: Magnetic properties, phosphodiester hydrolysis, DNA binding/cleavage, cytotoxicity and catecholase activity. Polyhedron 164:202–218. https://doi.org/10.1016/j.poly.2019.02.015

2. Garcia-Bosch I, Karlin KD (2014) Copper Peroxide Bioinorganic Chemistry:

From Metalloenzymes to Bioinspired Synthetic Systems. In: PATAI'S Chemistry of Functional Groups. John Wiley & Sons, Ltd, Chichester, UK, pp 1–52

3. Neves A, Rossi LM, Bortoluzzi AJ, et al (2002) Catecholase Activity of a Series of Dicopper(II) Complexes with Variable Cu−OH(phenol) Moieties. Inorg Chem 41:1788–1794. https://doi.org/10.1021/ic010708u

4. Sathya V, Murali M (2018) Functional mimics of type-2 and type-3 copper oxidases: Self-assembled molecular association in mononuclear copper(II) complex enhances the catalytic activity. Inorg Chem Commun 92:55–59. https://doi.org/10.1016/j.inoche.2018.04.003

5. Banu KS, Chattopadhyay T, Banerjee A, et al (2009) Mono- and dinuclear manganese(III) complexes showing efficient catechol oxidase activity: syntheses, characterization and spectroscopic studies. Dalton Trans 8755. https://doi.org/10.1039/b902498k

6. Klabunde T, Eicken C, Sacchettini JC, Krebs B (1998) Crystal structure of a plant catechol oxidase containing a dicopper center. Nature Struct Biol 5:1084–1090. https://doi.org/10.1038/4193

7. Dey SK, Mukherjee A (2016) Catechol oxidase and phenoxazinone synthase: Biomimetic functional models and mechanistic studies. Coord Chem Rev 310:80–115. https://doi.org/10.1016/j.ccr.2015.11.002

8. Abu-Dief AM, Mohamed IMA (2015) A review on versatile applications of transition metal complexes incorporating Schiff bases. Beni-Suef Univ J Basic Appl Sci 4:119–133. https://doi.org/10.1016/j.bjbas.2015.05.004

9. Madalan AM, Ene CD (2018) Supramolecular rectangles and ladders constructed from Ni(II), Cu(II) and Zn(II) mononuclear complexes with bicompartmental ligands and 4-aminopyridine as tectons. Inorg Chim Acta 475:184–192. https://doi.org/10.1016/j.ica.2017.06.058

10. Cozzi PG (2004) Metal–Salen Schiff base complexes in catalysis: practical aspects. Chem Soc Rev 33:410–421. https://doi.org/10.1039/B307853C

11. Finelli A, Hérault N, Crochet A, Fromm KM (2018) Threading Salen-type Cu- and Ni-Complexes into One-Dimensional Coordination Polymers: Solution versus Solid State and the Size Effect of the Alkali Metal Ion. Cryst Growth Des 18:1215–1226. https://doi.org/10.1021/acs.cgd.7b01769

12. Eicken C, Zippel F, Büldt-Karentzopoulos K, Krebs B (1998) Biochemical and spectroscopic characterization of catechol oxidase from sweet potatoes (Ipomoea batatas) containing a type-3 dicopper center 1. FEBS Lett 436:293–299. https://doi.org/10.1016/S0014-5793(98)01113-2

13. Rompel A, Fischer H, Meiwes D, et al (1999) Substrate specificity of catechol oxidase from Lycopus europaeus and characterization of the bioproducts of enzymic caffeic acid oxidation 1. FEBS Lett 445:103–110. https://doi.org/10.1016/S0014-5793(99)00106-4

14. Thakurta S, Chakraborty J, Rosair G, et al (2009) The interplay of O–H···O hydrogen bonding in the generation of three new supramolecular complexes of Cu^{II}, Ni^{II} and Co^{III}: Syntheses, characterization and structural aspects. Inorg Chim Acta 362:2828–2836. https://doi.org/10.1016/j.ica.2009.01.002

15. Gomes L, Sousa C, Freire C, Castro B de (2000) Diaqua{6,6′-dimethoxy-2,2′-

[propane-1,3-diylbis(nitrilomethylidyne-N)]diphenolato-O, O′}nickel(II). Acta Crystallogr Sect C Cryst Struct Commun 56:1201–1203. https://doi.org/10.1107/S010827010001009X

16. Thakurta S, Butcher RJ, Gómez-García CJ, et al (2010) Synthesis, structural aspects and magnetic properties of an unusual 2D thiocyanato-bridged cobalt(II)–Schiff base network. Inorg Chim Acta 363:3981–3986. https://doi.org/10.1016/j.ica.2010.07.069

17. Basak T, Ghosh K, Gómez-García CJ, Chattopadhyay S (2018) Synthesis, structure and magnetic characterization of a dinuclear and two mononuclear iron(III) complexes with N,O-donor Schiff base ligands. Polyhedron 146:42–54. https://doi.org/10.1016/j.poly.2017.12.040

18. Banerjee S, Saha A (2016) A new end-on (μ-1,1) azido bridged $[Zn_2(L)_2(Na)N_3]$ n 1D chain derived from a trinuclear zinc complex: syntheses, crystal structures, photoluminescence properties and DFT study. J Coord Chem 69:3092–3106. https://doi.org/10.1080/00958972.2016.1226502

19. Banerjee S, Ghorai P, Sarkar P, et al (2020) A rare flattened tetrahedral Mn(II) salen type complex: Synthesis, crystal structure, biomimetic catalysis and DFT study. Inorg Chim Acta 499:119176. https://doi.org/10.1016/j.ica.2019.119176

20. Biswas D, Chakrabarty PP, Saha S, et al (2013) Ligand mediated structural diversity and role of different weak interactions in molecular self-assembly of a series of copper(II)–sodium(I) Schiff-base heterometallic complexes. Inorg Chim Acta 408:172–180. https://doi.org/10.1016/j.ica.2013.09.011

21. Chiboub Fellah FZ, Costes J-P, Dahan F, et al (2007) Varying the metal/metal

ratio in related Cu–Ca complexes. Polyhedron 26:4209–4215. https://doi.org/10.1016/j.poly.2007.05.019

22. Branzea DG, Madalan AM, Ciattini S, et al (2010) New heterometallic coordination polymers constructed from 3d–3d′ binuclear nodes. New J Chem 34:2479. https://doi.org/10.1039/c0nj00238k

23. Cai X, Ning H (2015) Crystal structure of di-μ-acetato-diacetatobis(μ-6,6′-dimethoxy-2,2′-{[(propane-1,3-diylbis(azanylylidene)]bis(methanylylidene)}diphenolato)tetrazinc. Acta Crystallogr Sect E Crystallogr Commun 71:m217–m218. https://doi.org/10.1107/S2056989015020551

24. Wang J-H, Yan P-F, Li G-M, et al (2010) N,N′-bis(2-hydroxy-3-methoxybenzylidene)-1,3-diaminopropane dimeric 4f and 3d–4f heterodinuclear complexes: Syntheses, crystal structures and magnetic properties. Inorg Chim Acta 363:3706–3713. https://doi.org/10.1016/j.ica.2010.05.030

25. Lee JH, Im SY, Lee SW (2018) Pd–Ln and Pt–Ln complexes of a bi-compartmental ligand: [MLn(L)$(NO_3)_3$] (M= Pd, Pt; Ln= Eu, Tb; H_2L= *N*, *N*′-bis(3-methoxysalicylidenimino-1,3-diaminopropane)). Inorg Chim Acta 474:89–95. https://doi.org/10.1016/j.ica.2018.01.020

26. Pasatoiu TD, Ghirri A, Madalan AM, et al (2014) Octanuclear [$Ni^{II}_4Ln^{III}_4$] complexes. Synthesis, crystal structures and magnetocaloric properties. Dalton Trans 43:9136–9142. https://doi.org/10.1039/C4DT00515E

27. Wang H (2009) Aqua{6,6′-dimethoxy-2,2′-[propane-1,3-diylbis(nitrilomethylidyne)]diphenolato}copper(II). Acta Crystallogr Sect E

Struct Reports Online 65:m1490–m1490. https://doi.org/10.1107/S1600536809042755

28. Roy S, Basak T, Khan S, et al (2017) A Combined Experimental and Theoretical Study on the Formation of a Cyclic Tetrameric Water Cluster and a Similar Type of Cyclic Cluster in Copper(II) Schiff Base Complexes. ChemistrySelect 2:9336–9343. https://doi.org/10.1002/slct.201701266

29. Cucos A, Ursu A, Madalan AM, et al (2011) Co-crystallization of coordination compounds through second-coordination sphere interactions. CrystEngComm 13:3756. https://doi.org/10.1039/c1ce05112a

30. Routaray A, Nath N, Maharana T, Sutar A kumar (2015) Synthesis and Immortal ROP of L -Lactide Using Copper Complex. J Macromol Sci Part A 52:444–453. https://doi.org/10.1080/10601325.2015.1029370

31. Sheldrick GM (2015) SHELXT – Integrated space-group and crystal-structure determination. Acta Crystallogr Sect A Found Adv 71:3–8. https://doi.org/10.1107/S2053273314026370

32. Dolomanov O V., Bourhis LJ, Gildea RJ, et al (2009) OLEX2 : a complete structure solution, refinement and analysis program. J Appl Crystallogr 42:339–341. https://doi.org/10.1107/S0021889808042726

33. Routaray A, Nath N, Maharana T, et al (2016) Salicylaldimine Copper(II) complex catalyst: Pioneer for ring opening Polymerization of Lactide. J Chem Sci 128:883–891. https://doi.org/10.1007/s12039-016-1091-3

34. Nakamoto K (2008) Infrared and Raman Spectra of Inorganic and Coordination

Compounds. John Wiley & Sons, Inc., Hoboken, NJ, USA

35. Maurya RC, Patel P, Rajput S (2003) Synthesis and Characterization of *N*-(*o*-Vanillinidene)-*p*-anisidine and *N*,*N*′-bis(*o*-Vanillinidene)ethylenediamine and Their Metal Complexes. Synth React Inorg Met Chem 33:817–836. https://doi.org/10.1081/SIM-120021648

36. Banu KS, Mukherjee M, Guha A, et al (2012) Dinuclear copper(II) complexes: Solvent dependent catecholase activity. Polyhedron 45:245–254. https://doi.org/10.1016/j.poly.2012.06.087

37. Chattopadhyay T, Mukherjee M, Mondal A, et al (2010) A Unique Nickel System having Versatile Catalytic Activity of Biological Significance. Inorg Chem 49:3121–3129. https://doi.org/10.1021/ic901546t

38. Banu KS, Chattopadhyay T, Banerjee A, et al (2008) Catechol Oxidase Activity of a Series of New Dinuclear Copper(II) Complexes with 3,5-DTBC and TCC as Substrates: Syntheses, X-ray Crystal Structures, Spectroscopic Characterization of the Adducts and Kinetic Studies. Inorg Chem 47:7083–7093. https://doi.org/10.1021/ic701332w

39. Banu KS, Chattopadhyay T, Banerjee A, et al (2009) Catechol oxidase activity of dinuclear copper(II) complexes of Robson type macrocyclic ligands: Syntheses, X-ray crystal structure, spectroscopic characterization of the adducts and kinetic studies. J Mol Catal A Chem 310:34–41. https://doi.org/10.1016/j.molcata.2009.05.016

40. Adak P, Mondal A, Chattopadhyay SK (2020) Manganese(II) complex of an oxygen–nitrogen donor Schiff base ligand showing efficient catechol oxidase

activity: synthesis, spectroscopic and kinetic study. New J Chem 44:3748–3754. https://doi.org/10.1039/C9NJ04591K

41. Solomon EI, Sundaram UM, Machonkin TE (1996) Multicopper Oxidases and Oxygenases. Chem Rev 96:2563–2606. https://doi.org/10.1021/cr950046o

42. Güell M, Siegbahn PEM (2007) Theoretical study of the catalytic mechanism of catechol oxidase. JBIC J Biol Inorg Chem 12:1251–1264. https://doi.org/10.1007/s00775-007-0293-z

43. Kaizer J, Baráth G, Csonka R, et al (2008) Catechol oxidase and phenoxazinone synthase activity of a manganese(II) isoindoline complex. J Inorg Biochem 102:773–780. https://doi.org/10.1016/j.jinorgbio.2007.11.014

44. Blay G, Fernández I, Pedro JR, et al (2006) Chemistry and reactivity of dinuclear manganese oxamate complexes: Aerobic catechol oxidation catalyzed by high-valent bis(oxo)-bridged dimanganese(IV) complexes with a homologous series of binucleating 4,5-disubstituted-o-phenylenedioxamate ligands. J Mol Catal A Chem 250:20–26. https://doi.org/10.1016/j.molcata.2006.01.021

45. Hitomi Y, Ando A, Matsui H, et al (2005) Aerobic Catechol Oxidation Catalyzed by a Bis(μ-oxo)dimanganese(III,III) Complex via a Manganese(II)−Semiquinonate Complex. Inorg Chem 44:3473–3478. https://doi.org/10.1021/ic050109d

46. Mukherjee S, Weyhermüller T, Bothe E, et al (2004) Dinuclear and mononuclear manganese(IV)-radical complexes and their catalytic catecholase activity. Dalton Trans 3842–3853. https://doi.org/10.1039/B410842F

47. Doctrow SR, Huffman K, Marcus CB, et al (2002) Salen−Manganese Complexes as Catalytic Scavengers of Hydrogen Peroxide and Cytoprotective Agents: Structure−Activity Relationship Studies. J Med Chem 45:4549–4558. https://doi.org/10.1021/jm020207y

48. Prasad RV, Thakkar NV (1994) Study of cobalt complexes as catalysts in the decomposition of hydrogen peroxide. J Mol Catal 92:9–20. https://doi.org/10.1016/0304-5102(94)00063-8

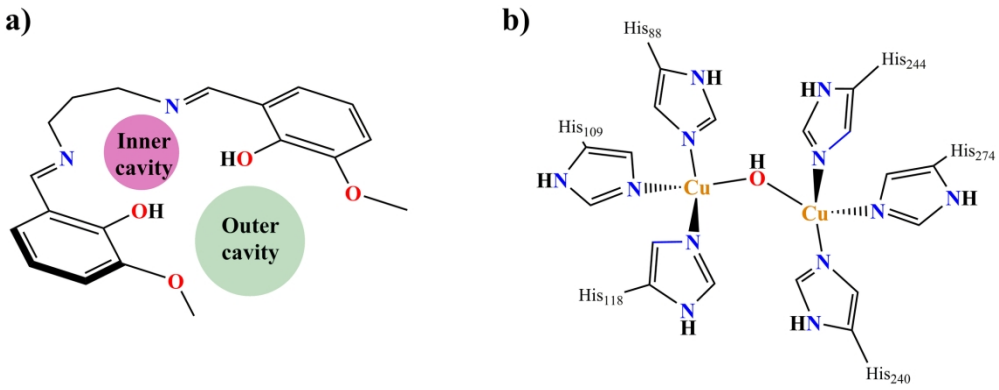

Fig. 1. Coordination environment resemblance between the bicompartmental ligand H_2L (a) and the active site of catechol oxidase enzyme (b).

197x76mm (300 x 300 DPI)

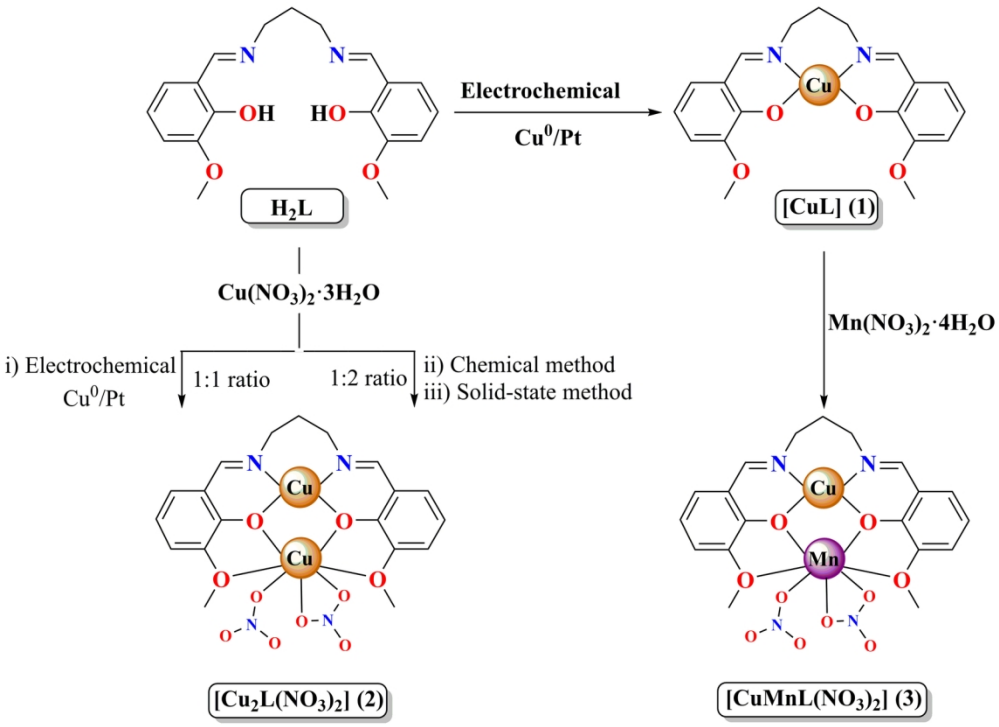

151x109mm (300 x 300 DPI)

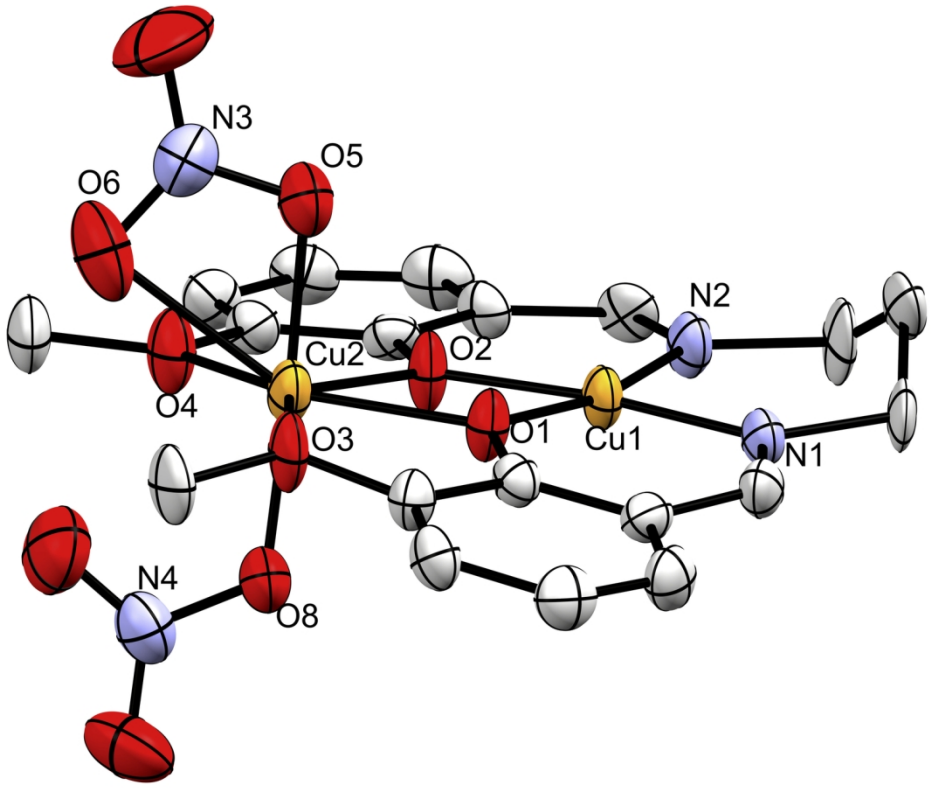

Fig. 2. ORTEP view (50% probability ellipsoids) and labelling scheme of the asymmetric unit for **2**.

149x119mm (300 x 300 DPI)

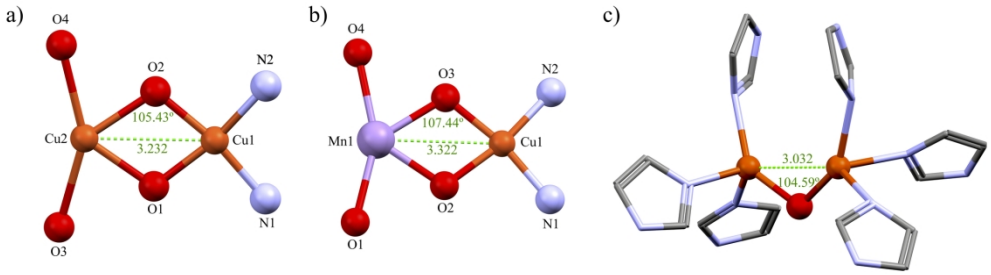

Fig. 3. Metal-metal distances and angles of dinuclear complexes, **2** (a) and **3** (b), and the coordination sphere of the dinuclear copper(II) centre of catechol oxidase from sweet potato in the *met* state (PDB ID: 1BT3) (c).

199x55mm (300 x 300 DPI)

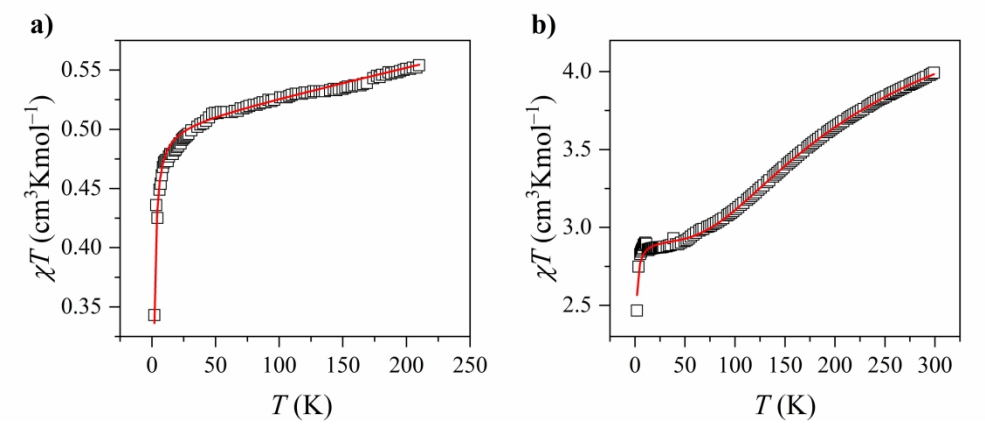

Fig. 4. Temperature dependence of χT for complexes a) **2** and b) **3**. The solid lines represent the fit of the data using the parameters described in the text.

272x114mm (300 x 300 DPI)

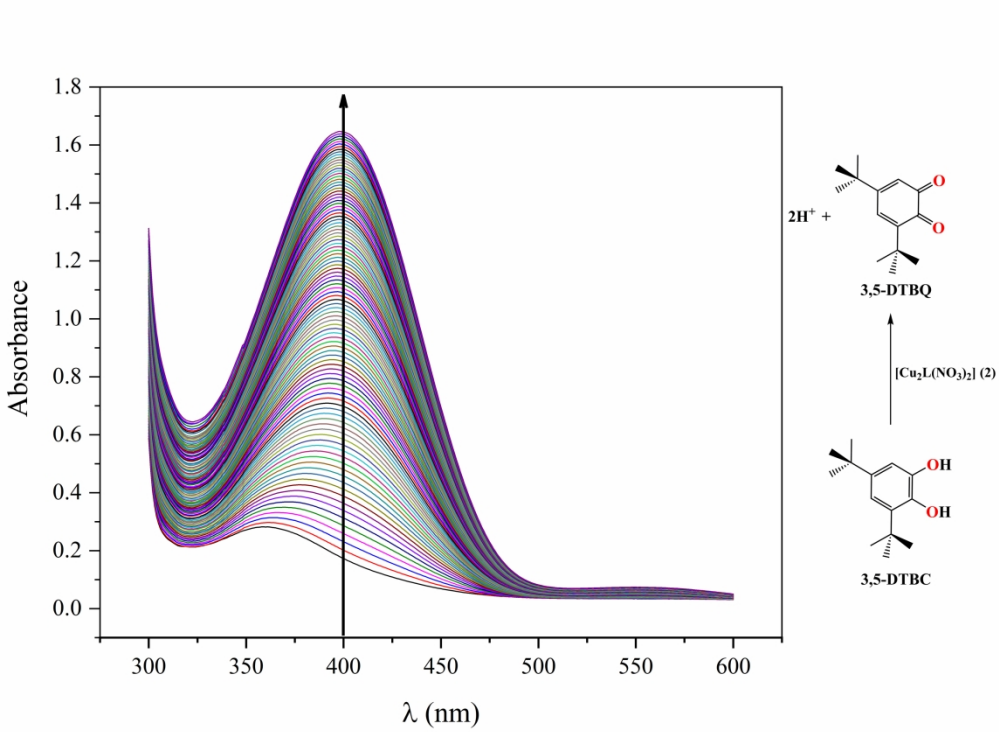

Fig. 5. Variation of 3,5-DTBQ absorbance at 400 nm after addition of complex **2**. The spectra were recorded at intervals of 60 seconds during 60 min.

272x208mm (300 x 300 DPI)

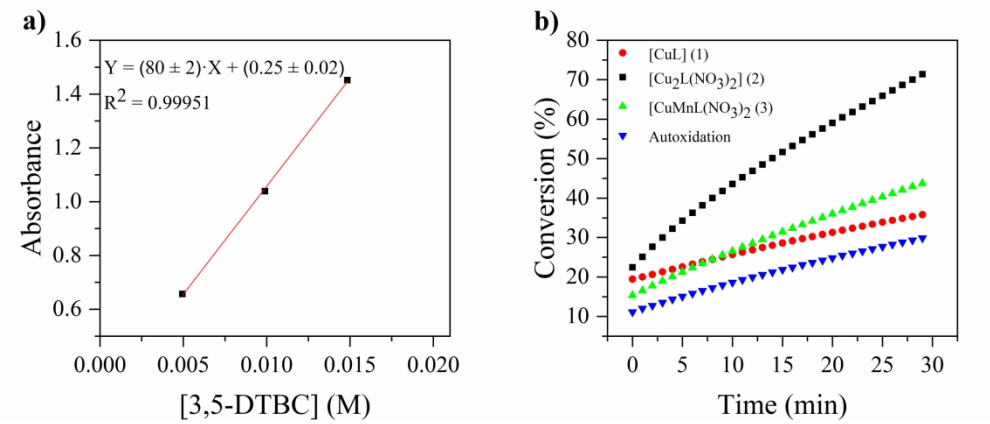

Fig. 6. a) Calibration curve of 3,5-DTBC. b) Percentage conversion of 3,5-DTBC to 3,5-DTBQ in the presence of the catalysts, **1** (red), **2** (green), **3** (black) and autoxidation (blue) during the first 30 min reaction time.

272x114mm (300 x 300 DPI)

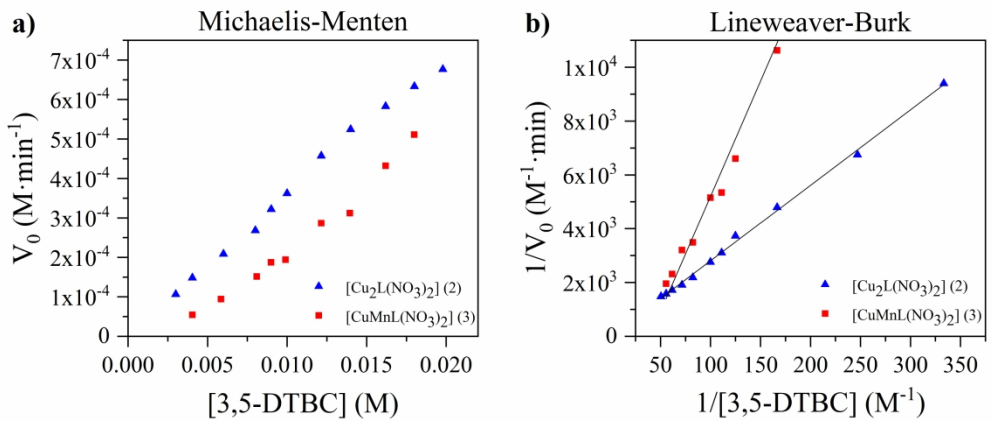

Fig. 7. a) Plot of initial rate vs. substrate concentration for the oxidation of 3,5-DTBC by complexes **2** (red) and **3** (blue). b) Lineweaver-Burk plot of complexes **2** (red) and **3** (blue).

272x114mm (300 x 300 DPI)

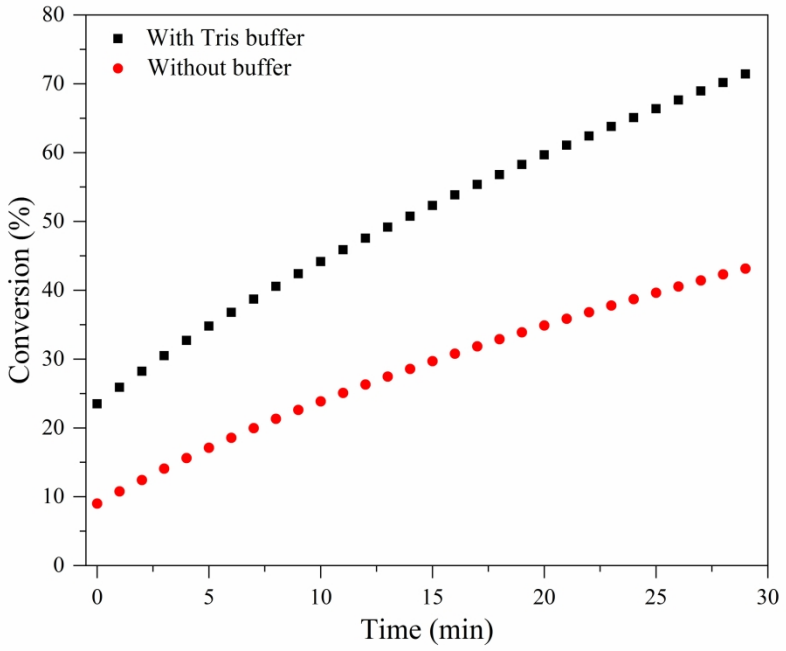

Fig. 8. Ratio of 3,5-DTBC conversion in Tris buffer medium (black) and without buffer (red) for **2**. Catalyst to 3,5-DTBC molar ratio 1:400.

272x208mm (300 x 300 DPI)

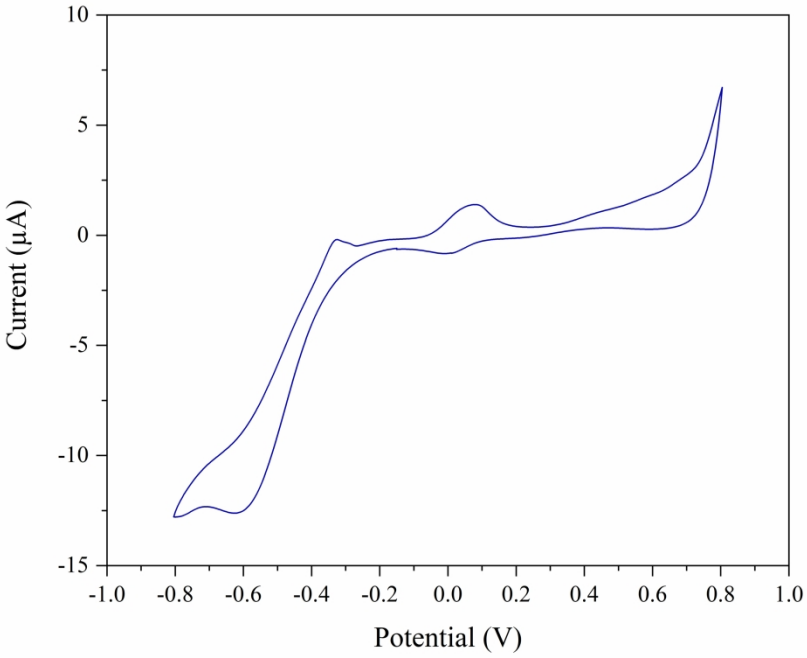

Fig. 9. Cyclic voltammogram of complex **2** in MeCN:H_2O (2:1) solution.

272x208mm (300 x 300 DPI)

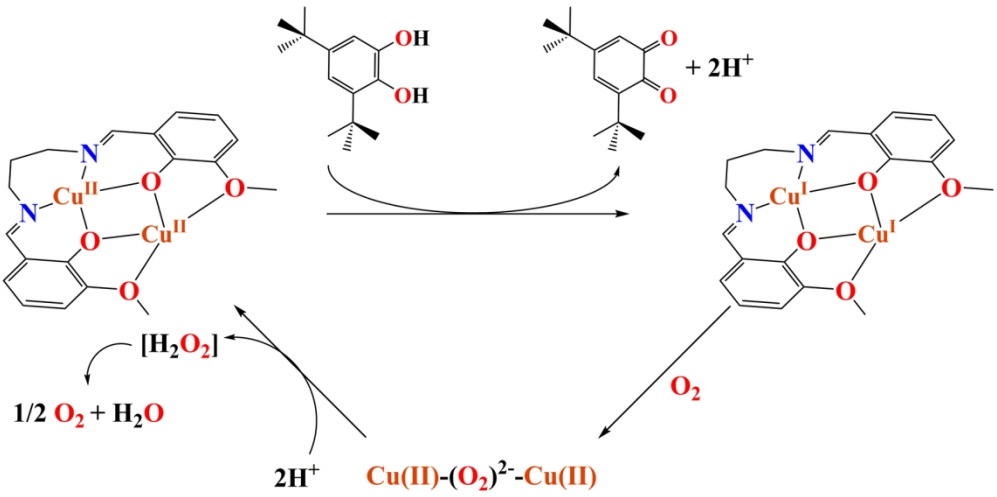

156x77mm (300 x 300 DPI)

Supplementary data

Design and catalytic studies of structural and functional models of the catechol oxidase enzyme

Aarón Terán*, Aida Jaafar, Ana E. Sánchez-Peláez, M. Carmen Torralba, Ángel Gutiérrez.

Departamento de Química Inorgánica, Facultad de Ciencias Químicas, Universidad Complutense de Madrid, Madrid 28040, Spain, aaronter@ucm.es

Table of content:

Table S1. Crystal data and structure refinement for $[Cu_2L(NO_3)_2]$.

Empirical formula	$C_{19}H_{20}Cu_2N_4O_{10}$
Formula weigh	591.47
Temperature	293(2) K
Wavelength	0.71073 Å
Crystal system	Triclinic
Space group	*P*–1
Unit cell dimensions	a = 8.4831(5) Å
	b = 11.1653(6) Å
	c = 11.4083(10) Å
	α = 83.326(6) °
	β = 84.244(6) °
	γ = 84.955(5) °
Volume	1064.63(13) $Å^3$
Z	2
Crystal size	0.20 × 0.13 × 0.05 mm
Density(calculated)	1.845 g/cm^3
m	2.065 mm^{-1}
Theta(max)	25.499°
Goodness- of- fit on F^2	1.118
Refinement	$R[F^2 > 2\sigma(F^2)]$= 0.0733
	$wR(F^2)$= 0.1831
Rint	0.0382
Largest diff. peak and hole	0.839, −0.569 eA^{-3}

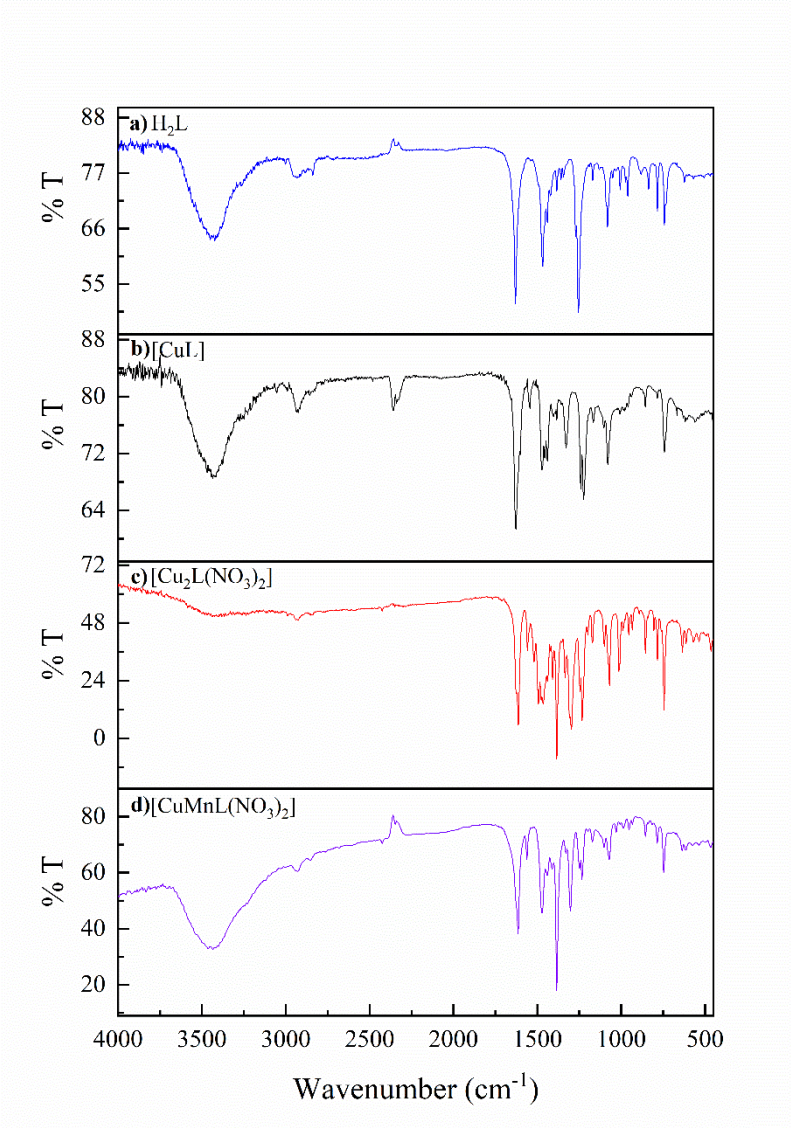

Fig. S1. Infrared KBr-dispersion spectra of a) H_2L, b) [CuL], c) $[Cu_2L(NO_3)_2)]$ and d) $[CuMnL(NO_3)_2)]$ compounds.

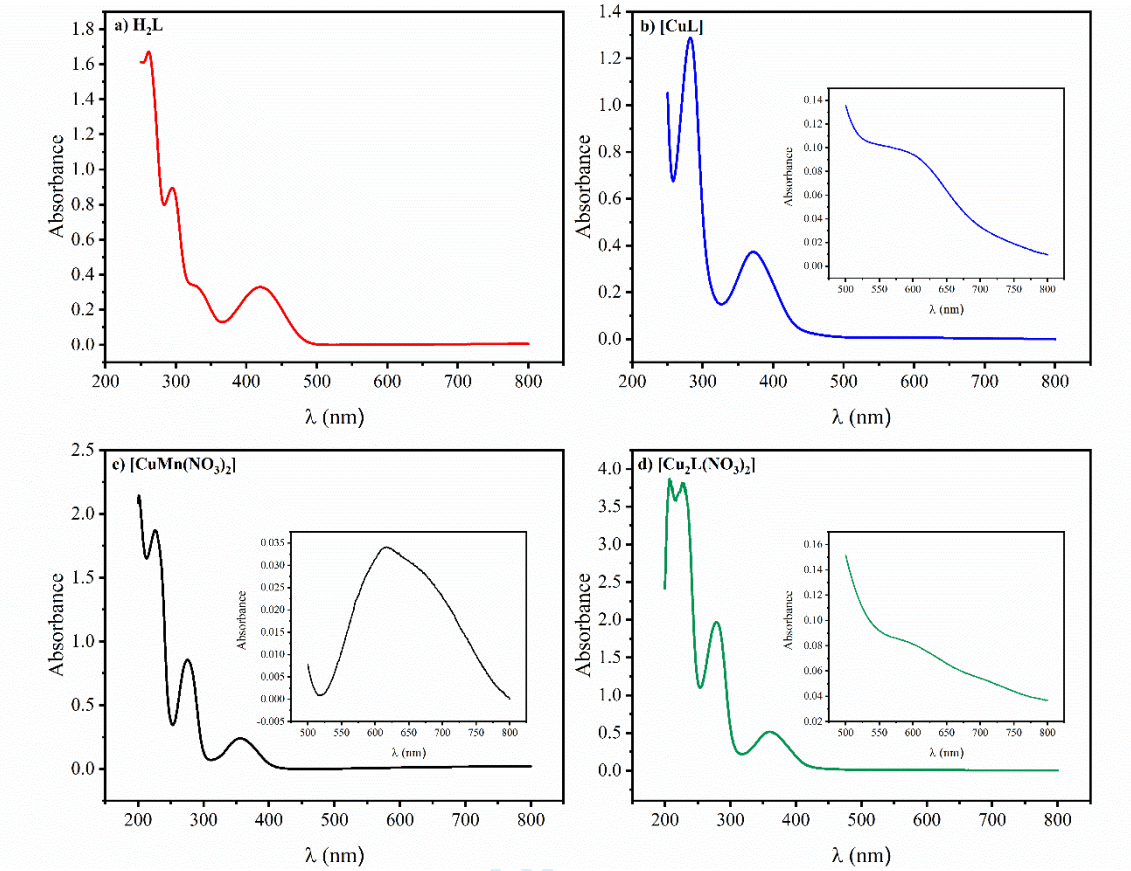

Fig. S2. Electronic spectra recorded in methanol solution of a) H_2L (1×10^{-4} M), b) [CuL] (5×10^{-4} and 5×10^{-5} M), c) $[CuMnL(NO_3)_2)]$ (10^{-3} and 8×10^{-5} M) and d) $[Cu_2L(NO_3)_2)]$ (10^{-3} and 8×10^{-5} M) compounds.

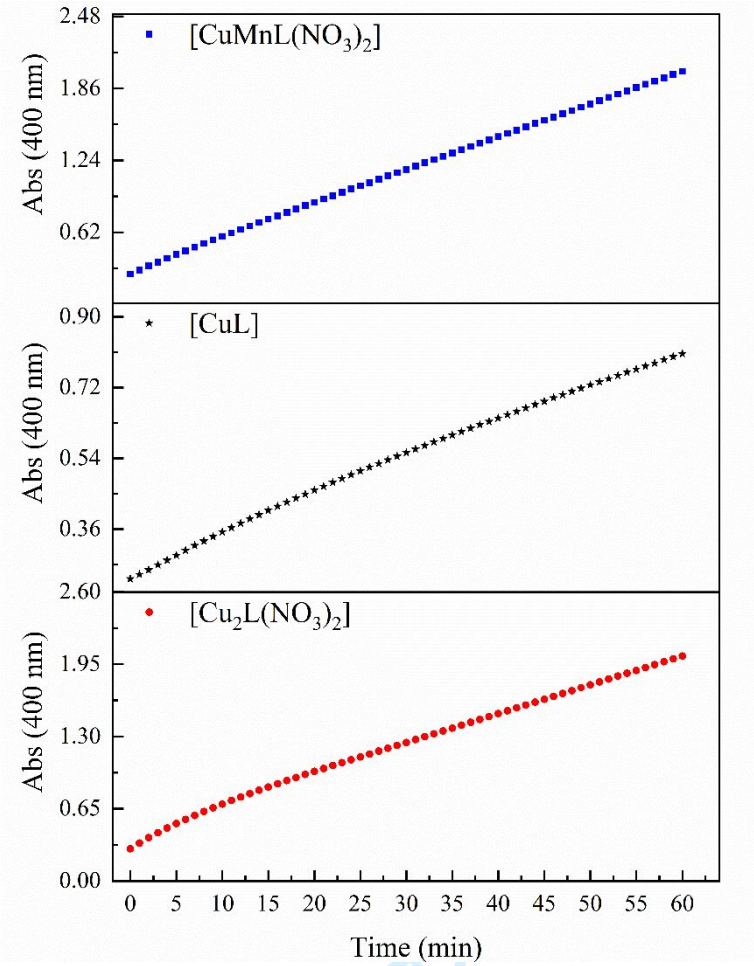

Fig. S3. Variation of 3,5-DTBQ absorbance at 400 nm after addition of $[CuMnL(NO_3)_2]$ (**blue**), [CuL] (**black**) and $[Cu_2L(NO_3)_2]$ (**red**) complexes. The spectra were recorded at intervals of 60 seconds during 60 min.

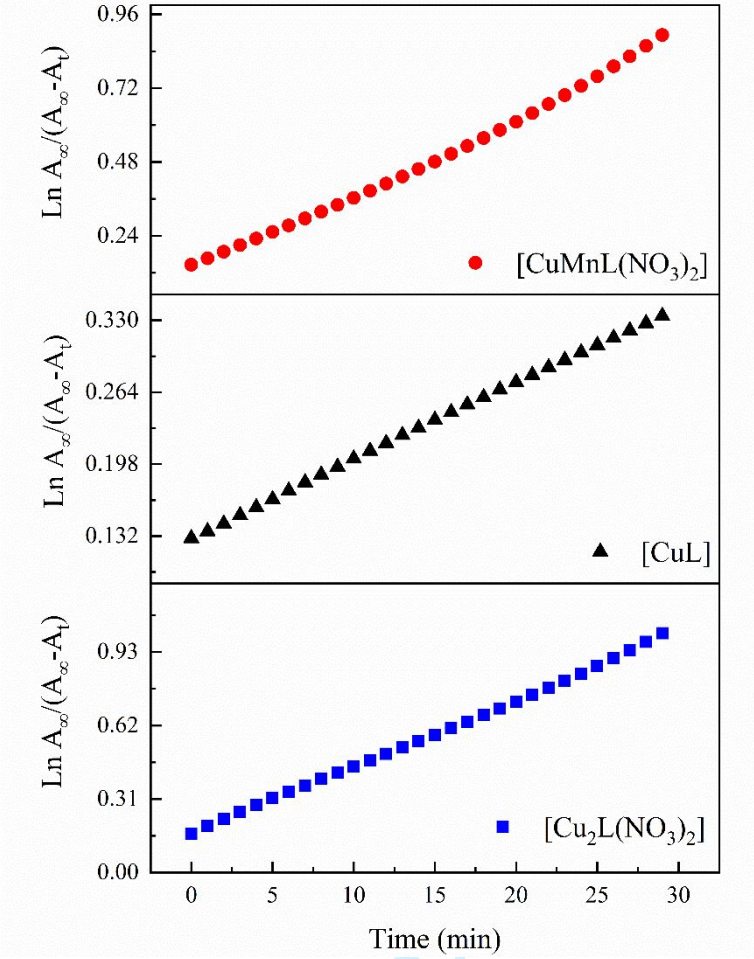

Fig. S4. First-order kinetic adjustment for absorbance data from $[CuMnL(NO_3)_2]$ (**red**), [CuL] (**black**) and $[Cu_2L(NO_3)_2]$ (**blue**) complexes.

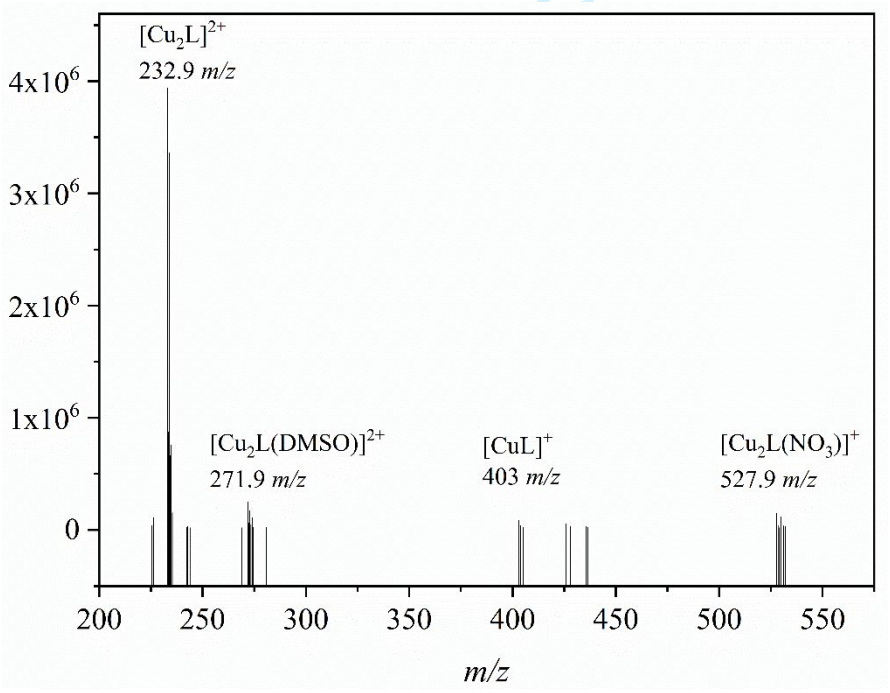

Fig. S5. ESI-MS spectrum of $[Cu_2L(NO_3)_2]$ complex in DMSO and MeOH.

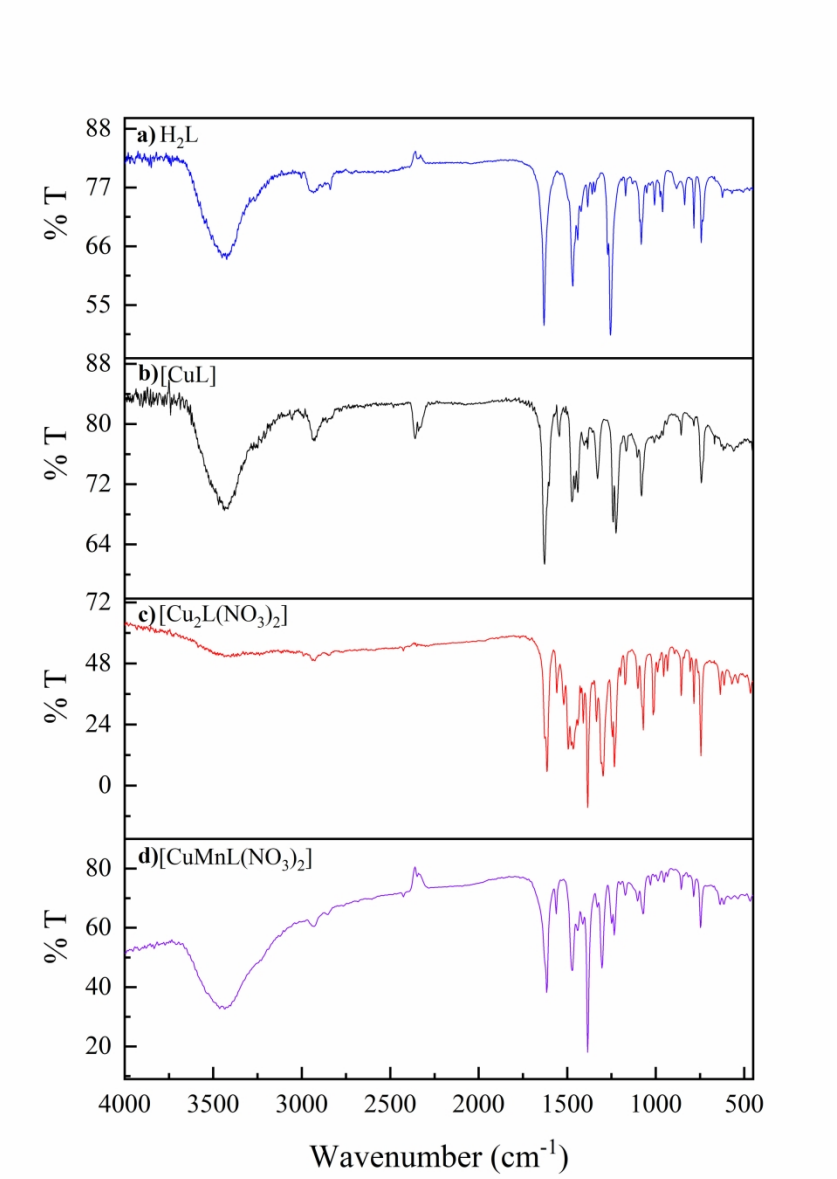

202x289mm (300 x 300 DPI)

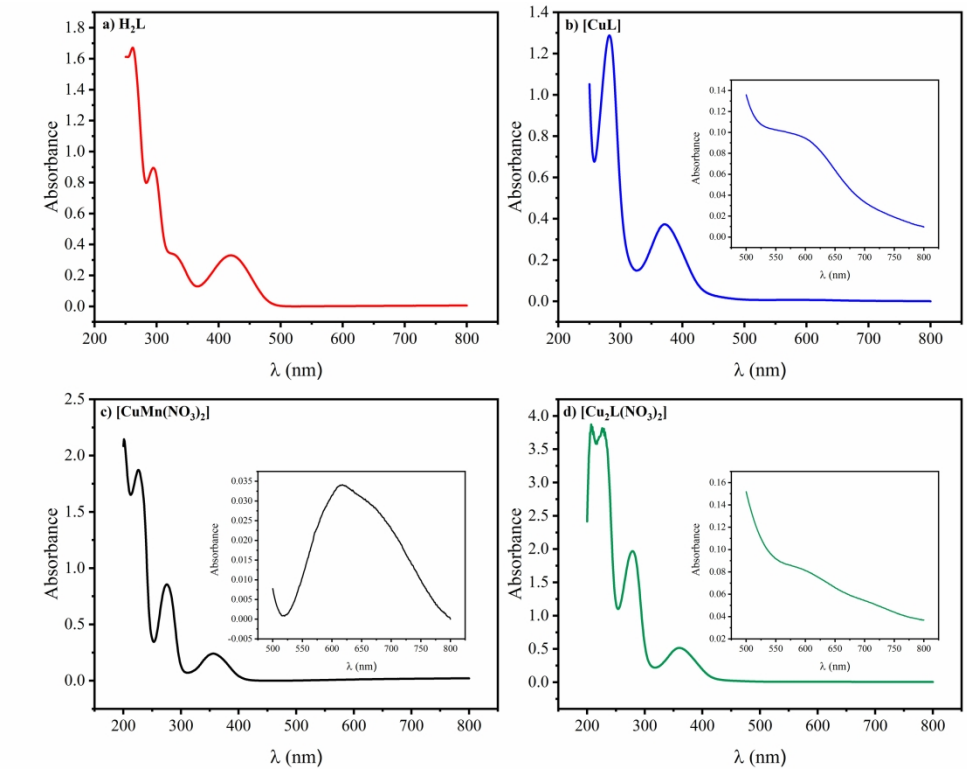

272x208mm (300 x 300 DPI)

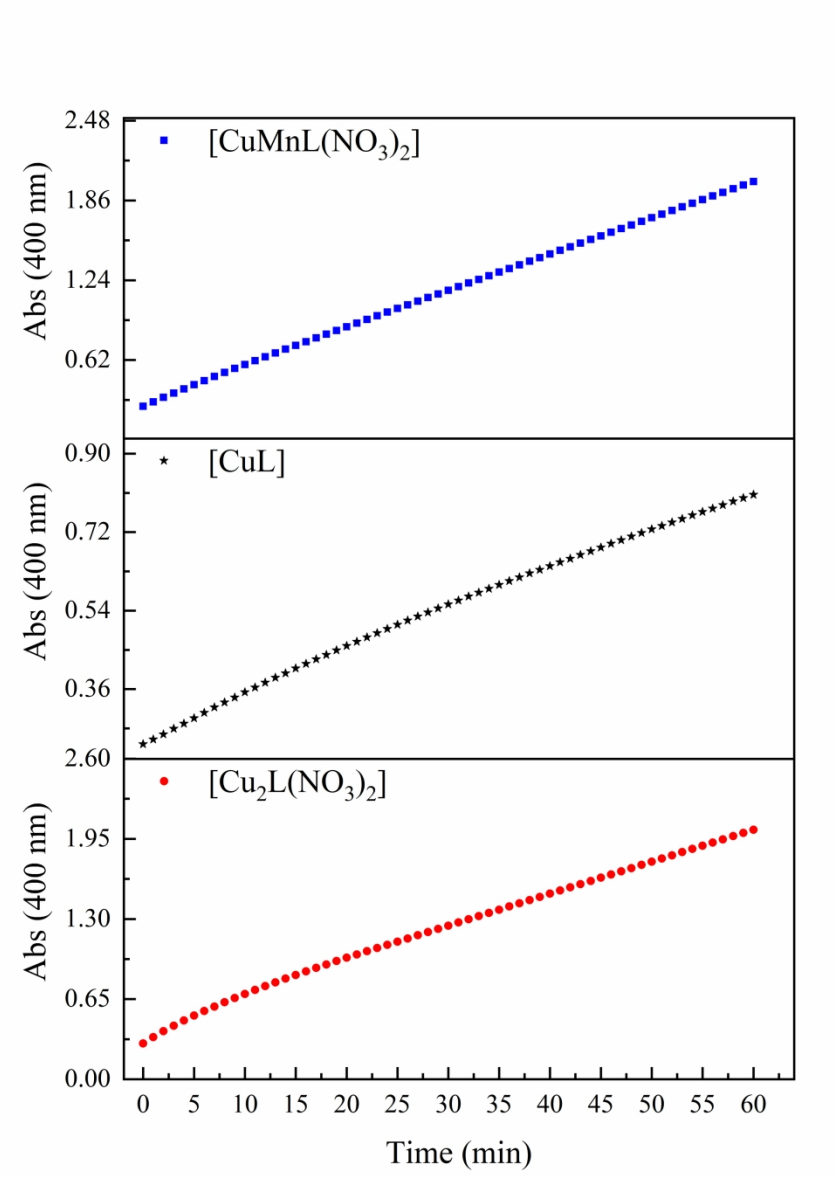

202x289mm (300 x 300 DPI)

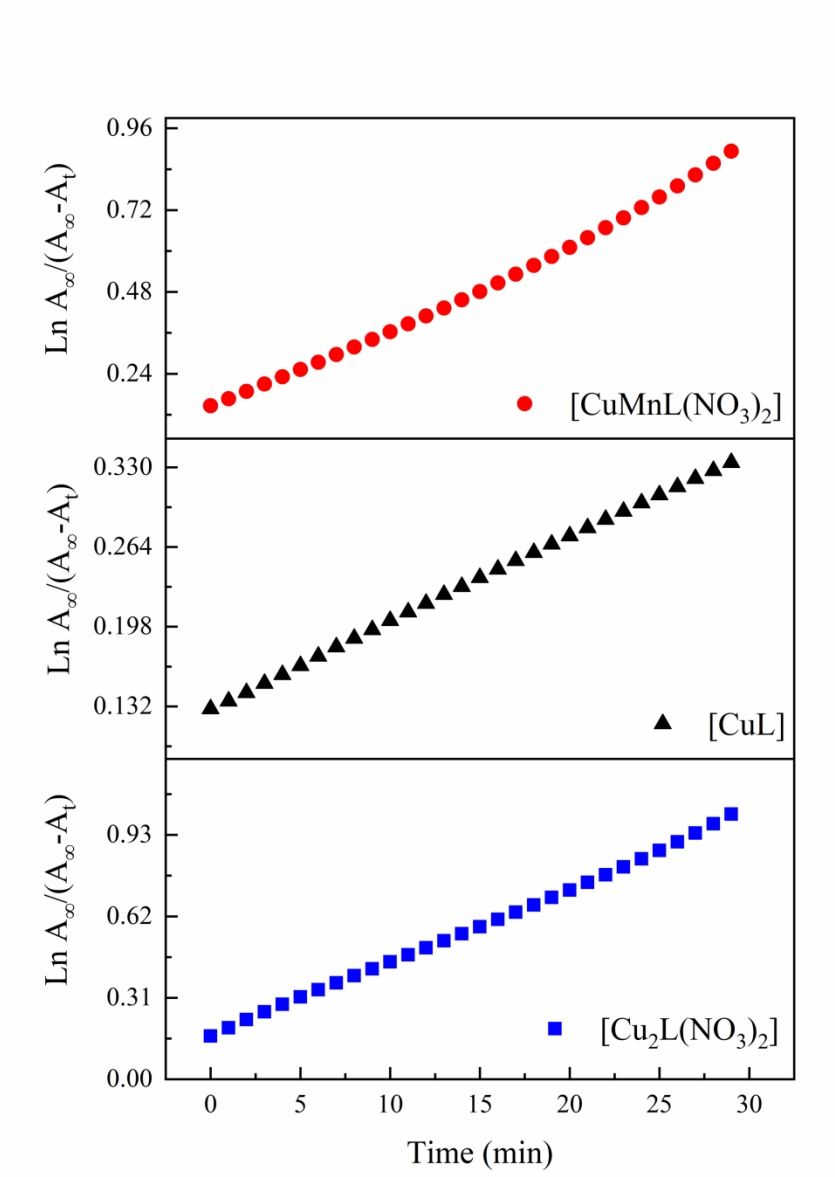

202x289mm (300 x 300 DPI)

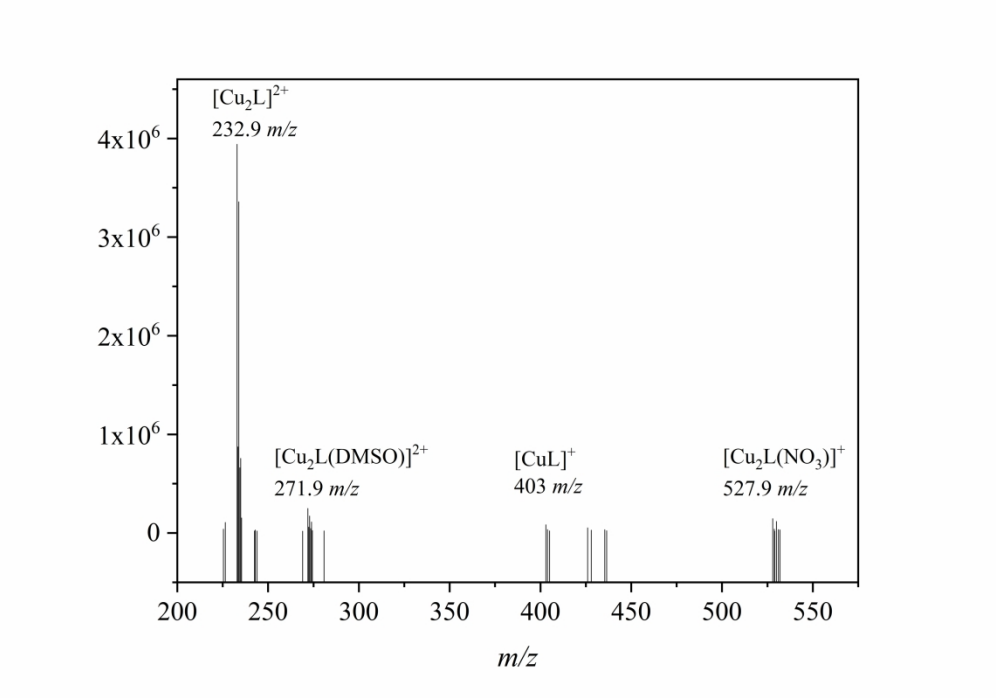

290x203mm (300 x 300 DPI)

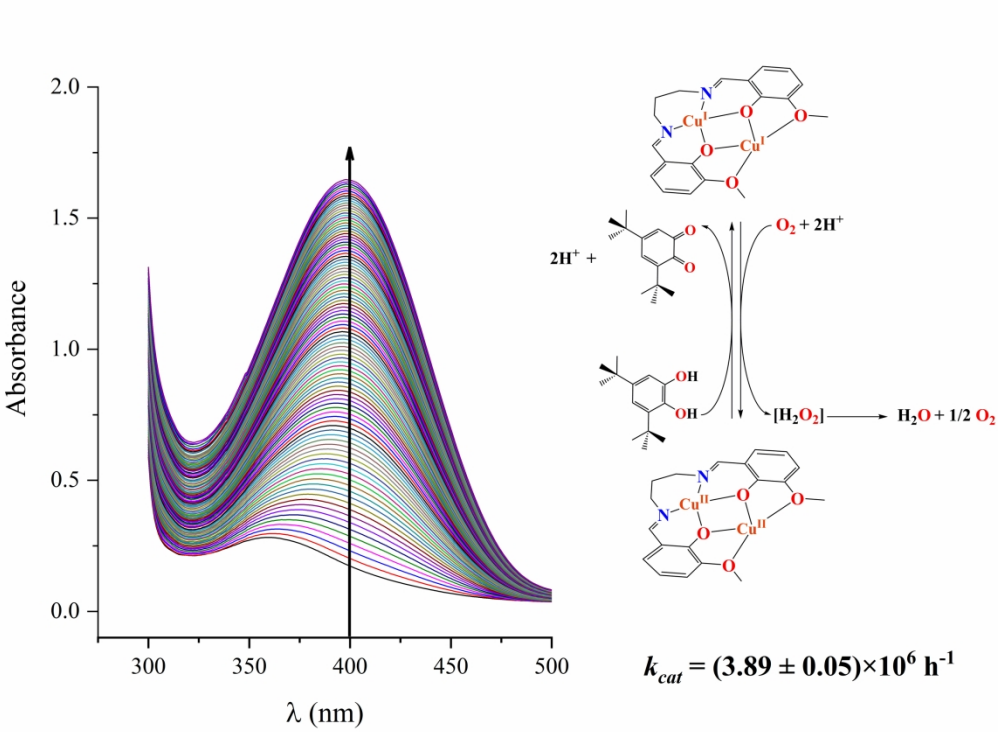

The design of three copper (II) derivatives, structurally analogous to the *type-3* catechol oxidase enzyme, using a bicompartmental Schiff base ligand, it has permitted to obtain complexes that can mimic the catalytic function of the enzyme. One of these compounds, dinuclear copper (II) complex, it shows the highest turnover value (k_{cat}) reported to date comparable to the enzyme itself.

272x208mm (300 x 300 DPI)

checkCIF/PLATON report

Structure factors have been supplied for datablock(s) I

THIS REPORT IS FOR GUIDANCE ONLY. IF USED AS PART OF A REVIEW PROCEDURE FOR PUBLICATION, IT SHOULD NOT REPLACE THE EXPERTISE OF AN EXPERIENCED CRYSTALLOGRAPHIC REFEREE.

No syntax errors found. CIF dictionary Interpreting this report

Datablock: I

```
Bond precision:  C-C = 0.0123 A          Wavelength=0.71073

Cell:          a=8.4831(5)       b=11.1653(6)     c=11.4083(10)
               alpha=83.326(6)   beta=84.244(6)   gamma=84.955(5)
Temperature:   293 K
```

	Calculated	Reported
Volume	1064.63(13)	1064.63(13)
Space group	P -1	P -1
Hall group	-P 1	-P 1
Moiety formula	C19 H20 Cu2 N4 O10	C19 H20 Cu2 N4 O10
Sum formula	C19 H20 Cu2 N4 O10	C19 H20 Cu2 N4 O10
Mr	591.49	591.47
Dx,g cm-3	1.845	1.845
Z	2	2
Mu (mm-1)	2.065	2.065
F000	600.0	600.0
F000’	601.55	
h,k,lmax	10,13,13	10,13,13
Nref	3963	3952
Tmin,Tmax	0.732,0.902	0.906,1.000
Tmin’	0.655	

```
Correction method= # Reported T Limits: Tmin=0.906 Tmax=1.000
AbsCorr = MULTI-SCAN

Data completeness= 0.997          Theta(max)= 25.499

R(reflections)= 0.0733( 2935)     wR2(reflections)= 0.1831( 3952)

S = 1.159                 Npar= 318
```

The following ALERTS were generated. Each ALERT has the format
test-name_ALERT_alert-type_alert-level.
Click on the hyperlinks for more details of the test.

Alert level B

```
PLAT930_ALERT_2_B FCF-based   Twin Law ( 0 0 1)[-1-1 5] Est.d BASF       0.15 Check
```

Alert level C

```
PLAT213_ALERT_2_C Atom C10            has ADP max/min Ratio .....        3.6 prolat
PLAT220_ALERT_2_C Non-Solvent  Resd 1  O   Ueq(max)/Ueq(min) Range        3.1 Ratio
PLAT241_ALERT_2_C High   'MainMol' Ueq as Compared to Neighbors of         O6 Check
PLAT241_ALERT_2_C High   'MainMol' Ueq as Compared to Neighbors of         O9 Check
PLAT242_ALERT_2_C Low    'MainMol' Ueq as Compared to Neighbors of         N3 Check
PLAT242_ALERT_2_C Low    'MainMol' Ueq as Compared to Neighbors of         N4 Check
PLAT341_ALERT_3_C Low Bond Precision on  C-C Bonds ...............    0.01231 Ang.
PLAT906_ALERT_3_C Large K Value in the Analysis of Variance ......      9.366 Check
PLAT910_ALERT_3_C Missing # of FCF Reflection(s) Below Theta(Min).         10 Note
```

Alert level G

```
PLAT003_ALERT_2_G Number of Uiso or Uij Restrained non-H Atoms ...         35 Report
PLAT012_ALERT_1_G No       _shelx_res_checksum Found in CIF ......     Please Check
PLAT083_ALERT_2_G SHELXL Second Parameter in WGHT  Unusually Large      10.17 Why ?
PLAT177_ALERT_4_G The CIF-Embedded .res File Contains DELU Records          1 Report
PLAT178_ALERT_4_G The CIF-Embedded .res File Contains SIMU Records          1 Report
PLAT199_ALERT_1_G Reported _cell_measurement_temperature ..... (K)        293 Check
PLAT200_ALERT_1_G Reported  _diffrn_ambient_temperature ..... (K)        293 Check
PLAT232_ALERT_2_G Hirshfeld Test Diff (M-X)  Cu2      --O6       .        7.2 s.u.
PLAT794_ALERT_5_G Tentative Bond Valency for Cu2       (II)      .       2.14 Info
PLAT860_ALERT_3_G Number of Least-Squares Restraints .............        350 Note
PLAT870_ALERT_4_G ALERTS Related to Twinning Effects Suppressed ..          ! Info
PLAT931_ALERT_5_G CIFcalcFCF  Twin Law ( 0 0 1)         Est.d BASF       0.15 Check
PLAT933_ALERT_2_G Number of OMIT Records in Embedded .res File ...          1 Note
```

```
   0 ALERT level A = Most likely a serious problem - resolve or explain
   1 ALERT level B = A potentially serious problem, consider carefully
   9 ALERT level C = Check. Ensure it is not caused by an omission or oversight
  13 ALERT level G = General information/check it is not something unexpected

   3 ALERT type 1 CIF construction/syntax error, inconsistent or missing data
  11 ALERT type 2 Indicator that the structure model may be wrong or deficient
   4 ALERT type 3 Indicator that the structure quality may be low
   3 ALERT type 4 Improvement, methodology, query or suggestion
   2 ALERT type 5 Informative message, check
```

checkCIF publication errors

Alert level A

```
PUBL004_ALERT_1_A  The contact author's name and address are missing,
           _publ_contact_author_name and _publ_contact_author_address.
PUBL005_ALERT_1_A  _publ_contact_author_email, _publ_contact_author_fax and
           _publ_contact_author_phone are all missing.
           At least one of these should be present.
PUBL006_ALERT_1_A  _publ_requested_journal is missing
           e.g. 'Acta Crystallographica Section C'
PUBL008_ALERT_1_A  _publ_section_title is missing. Title of paper.
PUBL009_ALERT_1_A  _publ_author_name is missing. List of author(s) name(s).
PUBL010_ALERT_1_A  _publ_author_address is missing. Author(s) address(es).
```

```
PUBL012_ALERT_1_A  _publ_section_abstract is missing.
            Abstract of paper in English.
```

```
   7 ALERT level A = Data missing that is essential or data in wrong format
   0 ALERT level G = General alerts. Data that may be required is missing
```

Publication of your CIF

You should attempt to resolve as many as possible of the alerts in all categories. Often the minor alerts point to easily fixed oversights, errors and omissions in your CIF or refinement strategy, so attention to these fine details can be worthwhile. In order to resolve some of the more serious problems it may be necessary to carry out additional measurements or structure refinements. However, the nature of your study may justify the reported deviations from journal submission requirements and the more serious of these should be commented upon in the discussion or experimental section of a paper or in the "special_details" fields of the CIF. *checkCIF* was carefully designed to identify outliers and unusual parameters, but every test has its limitations and alerts that are not important in a particular case may appear. Conversely, the absence of alerts does not guarantee there are no aspects of the results needing attention. It is up to the individual to critically assess their own results and, if necessary, seek expert advice.

If level A alerts remain, which you believe to be justified deviations, and you intend to submit this CIF for publication in a journal, you should additionally insert an explanation in your CIF using the Validation Reply Form (VRF) below. This will allow your explanation to be considered as part of the review process.

Validation response form

Please find below a validation response form (VRF) that can be filled in and pasted into your CIF.

```
# start Validation Reply Form
_vrf_PUBL004_GLOBAL
;
PROBLEM: The contact author’s name and address are missing,
RESPONSE: ...
;
_vrf_PUBL005_GLOBAL
;
PROBLEM: _publ_contact_author_email, _publ_contact_author_fax and
RESPONSE: ...
;
_vrf_PUBL006_GLOBAL
;
PROBLEM: _publ_requested_journal is missing
RESPONSE: ...
;
_vrf_PUBL008_GLOBAL
;
PROBLEM: _publ_section_title is missing. Title of paper.
RESPONSE: ...
;
_vrf_PUBL009_GLOBAL
;
PROBLEM: _publ_author_name is missing. List of author(s) name(s).
RESPONSE: ...
;
```

```
_vrf_PUBL010_GLOBAL
;
PROBLEM: _publ_author_address is missing. Author(s) address(es).
RESPONSE: ...
;
_vrf_PUBL012_GLOBAL
;
PROBLEM: _publ_section_abstract is missing.
RESPONSE: ...
;
# end Validation Reply Form
```

If you wish to submit your CIF for publication in Acta Crystallographica Section C or E, you should upload your CIF via the web. If you wish to submit your CIF for publication in IUCrData you should upload your CIF via the web. If your CIF is to form part of a submission to another IUCr journal, you will be asked, either during electronic submission or by the Co-editor handling your paper, to upload your CIF via our web site.

PLATON version of 03/05/2019; check.def file version of 29/04/2019

Datablock I - ellipsoid plot